Energy Conversion and Management 302 (2024) 118111

Contents lists available at ScienceDirect

Energy Conversion and Management

journal homepage: www.elsevier.com/locate/enconman

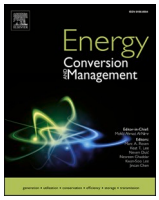

Control strategy and performance of a small-size thermally integrated Carnot battery based on a Rankine cycle and combined with district heating

Chiara Poletto [a,*], Olivier Dumont [b], Andrea De Pascale [a], Vincent Lemort [b], Saverio Ottaviano [a], Olivier Thomé [b]

[a] University of Bologna, Viale del Risorgimento 2, 40136 Bologna, Italy
[b] University of Liège, Allée de la Découverte 17, 4000 Liège, Belgium

ARTICLE INFO

Keywords:
Carnot battery
Rule-based control strategy
Energy management
Energy storage
Rankine cycle
District heating

ABSTRACT

To encourage decarbonization and promote a widespread penetration of renewable energy sources in all energy sectors, the development of efficient energy storage systems is essential. Interesting grid-scale electricity storage technologies are the Carnot batteries, whose working principle is based on storing electricity in the form of thermal energy. The charging phase is performed through a heat pump cycle, and the discharging phase is conducted through a heat engine. Since both thermal and electric energy flows are involved, Carnot batteries can be adopted to provide more flexibility in heat and power energy systems. To this aim, efficient scheduling strategies are necessary to manage different energy flows. In this context, this work presents a detailed rule-based control strategy to schedule the synergetic work of a 10-kWe reversible heat pump/organic Rankine cycle Carnot battery integrated to a district heating substation and a photovoltaic power plant, to satisfy a local user's thermal and electric demand. The coupling of a Carnot battery with a district heating substation allows for shaving the thermal demand peaks through the thermal energy stored in the Carnot battery storage, allowing for a down-sizing of the district heating substation, with a considerable reduction of the investment costs. Due to the multiplicity of the involved energy flows and the numerous modes of operation, a scheduling logic for the Carnot battery has been developed, to minimize the system operating costs, depending on the boundary conditions. To investigate the influence of the main system design parameters, a detailed and accurate model of the Carnot battery is adopted. Two variants of the reference system, with different heat pump cold source arrangements, are investigated. In the first case, the heat pump absorbs thermal energy from free waste heat. In the second case, the heat pump cold source is the return branch of the district heating substation. The simulation results show that, in the first case, the Carnot battery allows the downsizing of the district heating substation by 47 %, resulting in an annual gain of more than 5000 €. About 70 % of the economic benefit is due to the possibility of reducing the power size of the district heating substation, which can be from 300 to more than 500 kW. The payback period is estimated to be lower than 9 years, while in the second case, the Carnot battery is not able to provide a gain. Eventually, the influence of some parameters, such as the photovoltaic power plant surface, the storage volume, the electricity price profile and the reversible heat pump/organic Rankine cycle specific investment cost, on the techno-economic performance of the system, is investigated through a wide sensitivity analysis. According to the results, the photovoltaic panels surface does not significantly affect the economic gain, while the storage capacity strongly affects the system scheduling and the operating costs. Indeed, it is possible to identify that 13 m^3 is the size of the storage volume that minimizes the payback period to 8.22 years, for the considered application. An increase in the electricity price without an increase in the thermal energy price leads to a decrease in economic gain because the benefit brought by the downsizing of district heating is less significant on the economic balance. The specific investment cost of the reversible heat pump/organic Rankine cycle does not influence the operating cost; thus, it does not change the Carnot battery management, nor the economic gain. The specific investment cost affects the payback period, which increases from 8.6 years for a specific cost of 2000 €/kWe to 15.7 years for a specific cost of 5000 €/kWe.

* Corresponding author.
E-mail address: chiara.poletto3@unibo.it (C. Poletto).

https://doi.org/10.1016/j.enconman.2024.118111
Received 12 October 2023; Received in revised form 21 December 2023; Accepted 15 January 2024
Available online 26 January 2024
0196-8904/© 2024 The Author(s). Published by Elsevier Ltd. This is an open access article under the CC BY-NC-ND license (http://creativecommons.org/licenses/by-nc-nd/4.0/).

Nomenclature

Symbols

A	Area (m^2)
C	Cost (€)
COP	Coefficient of Performance (-)
c_p	Specific heat const. pressure (kJ/kg K)
E	Electric Energy (kWh)
I	Investment cost (€)
M	Mass (kg)
$\dot{m}$	Mass flow rate (kg/s)
n	Number (-)
Q	Thermal Energy (kWh)
$\dot{Q}$	Thermal Power (kW)
r	Discount Rate (-)
T	Temperature (°C)
U	Heat exchange coefficient (kW/m^2K)
V	Volume (m^3)
$\dot{W}$	Electric Power (kW)

Greek

α	Diffusivity coefficient (m^2/s)
γ	Self-consumption/production rate (%)
Δ	Difference (-)
Δprice	Price difference (€/kWh)
Δt	Time step (s)
Δx	Storage layer thickness (m)
η	Efficiency (%)

Subscripts

amb	ambient
ava	available
ave	average
CB2dem	from the CB to the demand
ch	charge
cons	consumption
dem	demand
dis	discharge
DH2HP	from DH to HP
el	electricity
fee	fee
grid	grid
i	i-th
max	maximum
min	minimum
nom	nominal
prod	production
pur	purchase
Q	thermal energy
r	discounted rate
ref	reference
ren	renewable
sale	sale
selfcons	self-consumption
sto	storage
sub	substation
surplus	surplus
wCB	with CB
woCB	without CB

Acronyms

ACAES	Adiabatic CAES
CAES	Compressed Air Energy Storage
CB	Carnot Battery
DH	District Heating
DPB	Discounted Payback
EES	Electric Energy Storage
HP	Heat Pump
H	High Temperature
LAES	Liquified Air Energy Storage
LT	Low Temperature
ORC	Organic Rankine Cycle
PB	Payback
PHES	Pumped Hydro Energy Storage
PTES	Pumped Thermal Energy Storage
PV	Photovoltaic
RES	Renewable Energy Sources
TES	Thermal Energy Storage
TI-PTES	Thermally Integrated PTES

1. Introduction

The decarbonization of the energy sector is among the main goals the International Energy Agency has set to reach within 2050 [1], in line with the Paris Agreement objective to limit the global temperature increase to 1.5 °C [2]. A deep penetration of renewable energy sources (RES) and a profound transformation of all the energy sectors are necessary to replace the fossil fuel-based energy supply, to reach 90 % carbon neutrality by 2050 [3]. Nowadays, the increasing fuel cost is resulting in a decrease in the ratio between the costs of electricity produced from renewables and fossil fuels [4]. However, the intrinsic instability and fluctuations of RES require a strong development of strategies to improve the match between renewable energy production and the users' demand. To this purpose, energy storage technologies gain primary importance as a solution to decouple energy production and demand over time.

1.1. Context

Different technologies have been proposed for Electric Energy Storage (EES), i.e.: electrochemical batteries [5], supercapacitors [6], flywheels [7], and hydrogen storage technologies coupled with fuel cell systems [8]. Other EES technologies are Pumped Hydro Energy Storage (PHES) [9], Compressed Air Energy Storage (CAES) [10], and its upgraded technology, named Adiabatic Compressed Air Energy Storage (ACAES) [11], which uses separate mechanical and thermal energy storages to increase the efficiency up to 70 %, as reviewed by Vecchi et al. [3]. Carnot batteries (CBs) can be classified as (i) Liquified Air Energy Storage (LAES) [12], in which the electric input is used to compress air that is then cooled down, until liquefaction occurs, and expanded to be stored at atmospheric pressure; (ii) Pumped Thermal Energy Storage (PTES) [13], based on Rankine or Brayton heat engines. However, the only grid-scale (long duration, from 4 to 8 h) EES technology, which has since now demonstrated techno-economic feasibility, is PHES [13]. Indeed, as the long duration results in extremely low power-to-capacity ratios (kW/kWh), the storage technology must be as cheap as possible. However, most of the grid-scale non-PHES solutions, like lithium batteries, shows remarkably high cost-per-capacity unit, which prevents them from being affordable for low power-to-capacity ratio applications. Furthermore, according to Gimeno-Gutiérrez and Lacal-Arántegui [14], PHES easily-exploitable additional capacity is nearly exhausted, so it is necessary to find valuable alternatives. CAES and ACAES technologies are drawing increasing attention due to the very inexpensive storage medium (usually air), but they require pre-

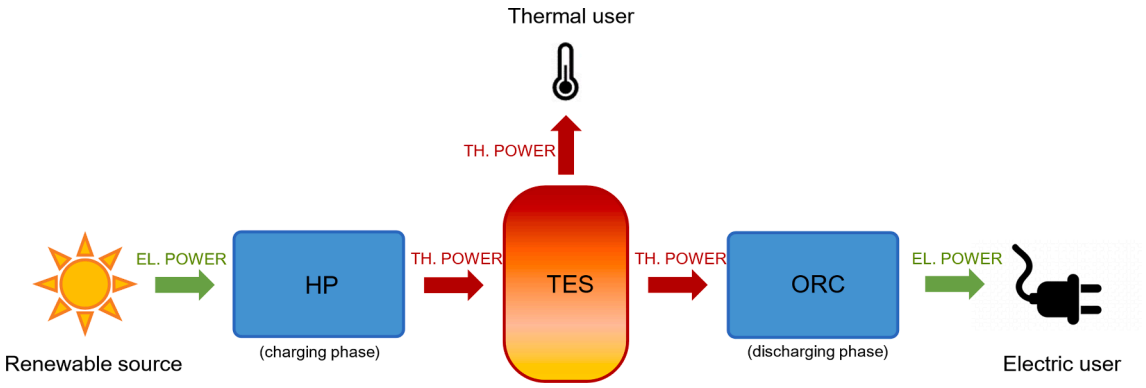

Fig. 1. General concept of Carnot battery.

existing reservoirs and caves, which are not available everywhere. In this context, as CBs are not constrained by geographical conditions, they represent an interesting alternative to PHES and CAES. In addition, although CBs might have lower conversion efficiencies, they present some features (low specific cost, long lifespan, the use of low environmental footprint materials, and the capability of being integrated with any type of waste heat source) that make them valuable grid-scale alternatives.

1.2. State of the art

A Carnot battery is an EES system, so it is primarily used to store electric energy. This means that there should always be at least an electric input and an electric output, which must be of the same order of magnitude. In the charging phase, the renewable electricity surplus is the energy input to create a thermal gradient, letting thermal energy flow from a low-temperature (LT) thermal energy source to a high-temperature (HT) thermal energy sink. The thermal energy is stored in a thermal energy storage (TES) until electric energy is not required. When the discharging phase occurs, the stored thermal energy is released from a HT source (which is the TES) to a LT sink, producing mechanical work, through a heat engine, which can be converted into electricity [13].

As the charging phase requires an electric input to create a thermal gradient, the availability of recoverable low-grade waste heat reduces the thermal lift (i.e., the temperature difference between the HT thermal energy reservoir and the LT thermal energy reservoir). Therefore, recoverable waste heat decreases the electrical energy needed in the heat pump cycle to obtain relatively high temperature thermal energy. In other words, the diversification of the temperature lift between the inverse cycle (charging phase) and the direct cycle (discharging phase), allows to improve conversion efficiencies [15], and thus the overall storage efficiency (also known as roundtrip efficiency) [16]. PTES integrated with low-temperature thermal energy sources, such as solar energy, district heating, and waste heat recovery, are called Thermally Integrated PTES (TI-PTES). Ökten and Kurşun [17] present a thermodynamic analysis on a TI-PTES combined with an absorption refrigeration cycle and they obtain a roundtrip efficiency of 142%. Frate et al. [18] propose a numerical model of a TI-PTES using Coolprop thermodynamic properties and they simulate a roundtrip efficiency of 130 % when working with the refrigerant R1233zd(E). Su et al. [19] develop mathematical models to compare the performance reachable with four CB configurations thermally integrated with geothermal energy. All the analysed configurations reach a heat-to-power efficiency higher than 100 %, but the most performing is assessed to be the flash heat pump-organic Rankine cycle configuration, with a COP of 6.13 and a heat-to-power efficiency of 137.13 %. Zhang et al. [20] evaluate the thermodynamic performance of a Rankine cycle-based CB thermally assisted by the steam extracted by a coal-fired power plant. They assess that the integration of the CB with the thermal power plant i) improves the CB roundtrip efficiency up to 114.67 % with a decrease of power generation efficiency of less than 3 percentage points, and ii) reduces the carbon emission by 1.26 %. Another way to introduce thermal integration is using the waste heat as HT source for the discharging phase, and the LT reservoir as energy storage, which stores thermal energy at temperatures below the ambient conditions [13]. Xia et al. [21] compare three different configurations of cold storage Rankine Carnot batteries. The results of this analysis show that including a recuperator in the vapour compression refrigeration unit and a preheater in the organic Rankine cycle unit improves the energy, exergy, and economic performance of the CB. A further original way to exploit a waste heat stream is proposed by Bellos [22] and it consists in feeding first the latent storage with the waste heat, and then the evaporator of the heat pump to enhance the charging phase performance. The performance improvement of the system suggested by Bellos ranges between 12.37 % and 173.58 % depending on the waste heat temperature.

Furthermore, as both thermal and electric energy flows are involved, CBs can be easily expanded from purely electrical energy storage to a heat and electricity storage and management energy system, allowing for a flexible sector coupling (Fig. 1). In this context, the integration of CBs into district heating (DH) networks introduces more flexibility and advantages even in thermal production/consumption [23]. A promising application of a CB integrated with DH is presented and widely discussed in this work.

PTES systems can be based on the direct/inverse Rankine cycle or the direct/inverse Brayton cycle. Although the roundtrip efficiencies are almost similar between Rankine and Brayton CBs, the characteristics of the two solutions are quite different.

In Rankine PTES, the charging and discharging phases are performed respectively by a vapour compression heat pump and a direct Rankine cycle. The heat pump cycle stores thermal energy exploiting an electric input to compress the working fluid to high pressure and temperature, and recovering the thermal energy released in the condensing transformation. The Rankine cycle, instead, is powered through the stored thermal energy, which is reconverted into mechanical energy, and then electricity, through a turbine or a volumetric expander [24]. Rankine PTES usually stores energy at lower temperatures than Brayton PTES with considerable advantages, namely fewer thermal losses, and the possibility of using less expensive materials for the machines and the reservoir. Concerning the suitable working fluid, in literature there are different solutions, including water vapour [25], organic fluids [16], transcritical CO_2 [26], and subcritical NH_3 [27]. Since the heat pump and the direct Rankine cycle show numerous similarities in terms of working fluid and main components, some works analyse Rankine PTES systems using the same machine (compressor/expander) and heat exchangers to perform both the charging and the discharging phases, with a considerable reduction of the investment costs [13]. This solution is named reversible heat pump/Rankine cycle system [26]. Yu et al. [28]

present a thermo-economic comparison among three Rankine-based CB systems, including a base configuration, a reversible configuration with two different machines for the charging and the discharging phases, and a reversible configuration using a dual-function machine. The results show that the third configuration, even if presenting lower power-to-power and exergy efficiencies than the first two, ensures the lowest levelized cost of storage, which is 12.3 % and 5.4 % lower than respectively the first and the second configurations.

Nowadays, only a few CB prototypes have been built and tested to demonstrate the performance and reliability of the system [29]. Although site-independent (unlike PHES and CAES) and with a long lifespan (unlike many chemical batteries), the high capital cost of the machines and especially of the storage is not an advantage in the CBs market competitiveness. Therefore, deeper investigation and research on the technology are necessary to find a compromise between performance, cost, and compactness.

Furthermore, when applied in integrated systems for storing renewable energy, CBs require the development of efficient scheduling strategies, to deal with different energy flows and manage the integrated system operation in each condition. Niu et al. [30] apply a multi-objective optimization model integrating a CB with solar collectors. They compare the results for a basic and a regenerated CB, and for different working fluids, during the summer and winter solstice days. The Authors have found out that there are optimal hot and cold reservoir temperatures and optimal combinations of working fluids for each of the two CB configurations, to maximize the roundtrip efficiency and minimize the levelized cost of the storage. Tassenoy et al. [31] propose a techno-economic assessment of a CB integrated with a photovoltaic (PV) power plant for electricity load-shifting of the renewable production, applied to an office building. They found out that the implementation of a CB in the studied case is not cost-effective. However, the CB was integrated only for electricity load-shifting. The cost-effectiveness of thermal energy load-shifting has not been investigated yet. The present work aims at extending the study [31] analysing the cost-effectiveness of a CB that covers the thermal energy demand peaks, allowing for thermal energy load-shifting. Lin et al. [32] propose a cross-border integrated energy system including a CB based on phase change material storage that can store electricity in the form of steam. The Authors have quantified a reduction of 28.57 % in the operating cost, 43.49 % in the carbon emission, and 16.49 % in the grid power purchase cost, compared to electric batteries in the case study of an industrial park. However, the Authors recommend the use of steam CB in integrated energy systems in scenarios with abundant renewable energy and low-grade heat availability. Scharrer et al. [33] present a control strategy for the operation of a reversible heat pump (HP)/organic Rankine cycle (ORC) CB, integrated with PV panels in a domestic application in a community with a varying number of houses. In this case, the CB is used only for electric load-shifting. Thus, a rule-based operation is implemented to charge the storage when a surplus of electricity is available and discharge it at night. Results show that increasing too much the PV size, and/or the storage capacity, is useless as soon as respectively the HP and the ORC work at their nominal conditions. The Authors also performed a financial analysis varying the feed-in-tariff and the thermal energy cost. Although interesting power-to-power efficiency values ($\approx$ 50 %), the feed-in tariff and the thermal energy costs should be almost null and coupled with high electricity prices, to provide savings per house up to 180 € per year, with an amortization period of 13 years. As in Scharrer et al. work, also in the present study a control strategy for the operation of a reversible HP/ORC is presented, but the CB is used mostly for thermal load-shifting, and secondarily for electric load-shifting, showing an interesting economic benefit and a lower amortization period. Therefore, the present work can be considered an extension of the analysis carried out in [33], filling the gap related to the possibility of using the CB for both thermal and electric load-shifting. Within the CHESTER project [34], a Compressed Heat Energy Storage (CHEST) is expected to be combined with the smart DH. As part of the CHESTER project, three case studies have been investigated considering different boundary conditions and including a comparison with other storage solutions, namely lead-acid batteries and a hydrogen storage system. They found out that the gain provided by the reduction of the imported electricity is negligible compared to the investment costs of the storage options, which is not always repaid by the increased profit. However, compared to the hydrogen solution, the CHEST system was demonstrated to be economically better by between 15 % and 50 % [35]. Within the same project, the electricity-only market and both the electricity and the heat markets are considered [36]. Results show that the scenario involving the heat exchange is more robust and may be less affected by competition from other storage facilities than the electricity-only, due to the multi-energy system integration.

According to the previous literature review and the Authors' best knowledge, the potential advantage of thermal energy load-shifting, has not been investigated yet in the previously published research. To fill this gap analysis, the integration of a reversible HP/ORC Carnot battery with DH is investigated in this study, and the benefit provided by the thermal demand peak shaving through the CB is assessed.

1.3. Contribution of this work

Based on the above literature review, to the Authors' best knowledge, few studies present a detailed control strategy to manage and schedule a CB operation in an integrated system, which aims at satisfying a user's thermal and electric demand. Therefore, as an original contribution to the current literature on the topic, this paper presents the techno-economic assessment of reversible HP/ORC Carnot battery integrated with a DH substation and a PV power plant, to satisfy a representative thermal and electric energy demand. The application to a university campus building, comprising laboratories and offices, is considered as test case. The CB coupling with a DH substation is interesting because the thermal energy stored in the TES can shave the thermal demand peaks, allowing the downsizing of the DH substation, with a considerable reduction of the investment costs.

A detailed rule-based control strategy has been implemented to schedule the CB operation by optimizing the actual work of the three main interacting sub-systems, namely the CB, the DH substation, and the PV power plant for a reference year operation. To this purpose, a detailed off-design model of an existing reversible HP/ORC kWe-size prototype CB [37], developed in a previous work [23] and improved with a stratified thermal energy storage tank model for the TES simulation, is employed in the control strategy. This study aims to assess the performance of the whole integrated system, under variable boundary conditions, during annual operation to maximize the economic gain due to the CB intervention. Two reference cases are analysed, differing one from the other only for the HP cold source, which is assumed to be free waste heat in the first case, and thermal energy provided by the DH in the second case. Furthermore, a sensitivity analysis, varying the PV panels surface, the storage volume, the electricity price profile, and the reversible HP/ORC specific cost of the investment, is conducted to observe how such parameters affect the system's yearly design, operation, and performance.

The paper is organized into two main sections, namely the methods and the discussion of the results. The methods section describes the main components of the system and the relationships among them, the CB management strategy, the hypothesis and boundary conditions of the two reference case studies, and the performance indicators. The results and discussion section presents the overall performance of the system in the two reference cases. Furthermore, some rules and hypotheses adopted in the control strategy are discussed, and a sensitivity analysis varying alternatively some key parameters is provided. Eventually, the conclusions section summarizes the main contribution and results of the current study, which provides guidelines to choose applications and optimally size a typical thermally integrated CB.

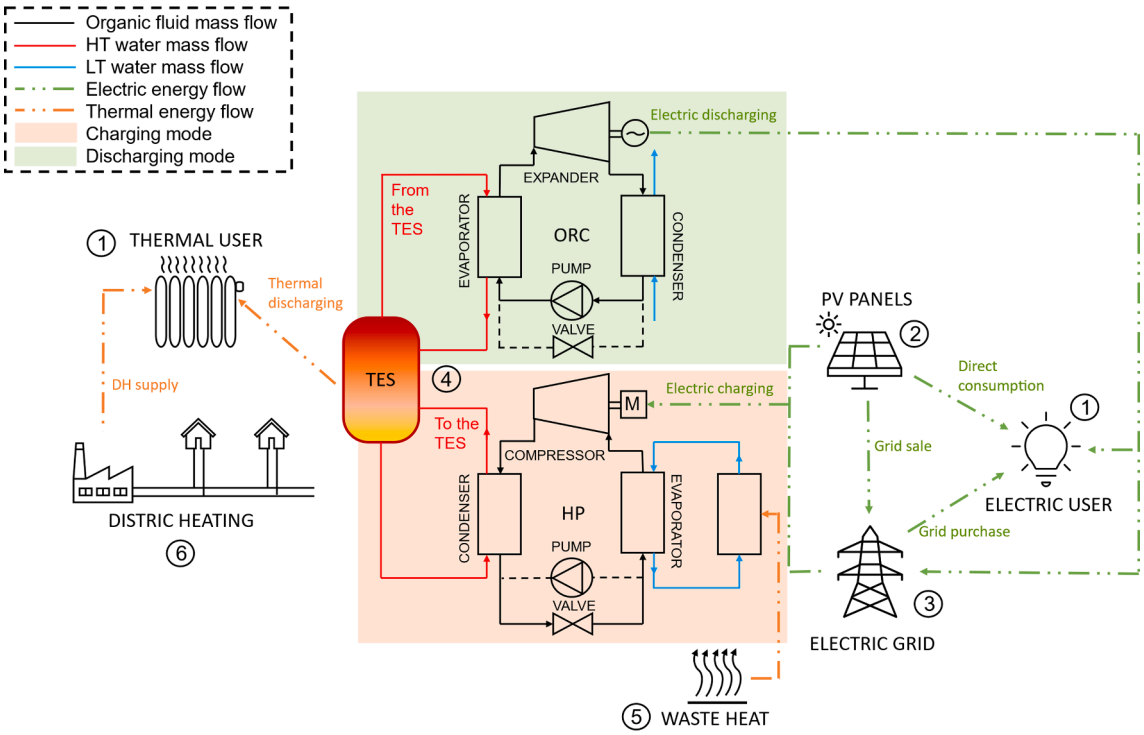

Fig. 2. The integrated energy system. The CB charging (HP) and discharging (ORC) modes are shown via separated subsystems for the sake of clarity in the figure, even if in the reference system the CB is a reversible HP/ORC loop.

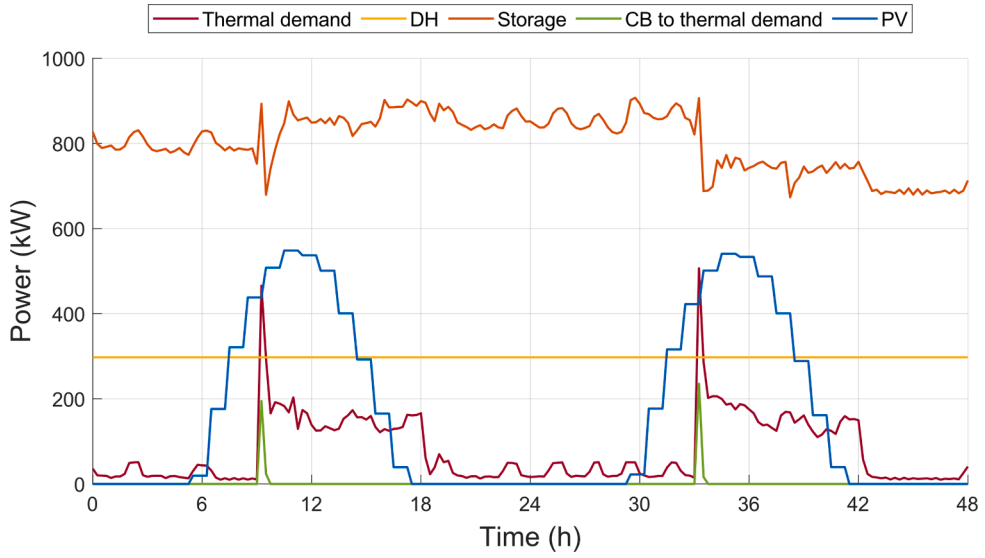

Fig. 3. Thermal power profiles for the reference application on two consecutive days in March, with the user thermal demand, the DH substation power size, the storage available thermal power (Eq. (12)), the thermal power provided by the CB TES to satisfy the thermal demand peaks and the PV electric production profile.

2. Materials and methods

The energy system proposed in this study is composed of a PV power plant and a DH substation adopted to cover a university campus building's thermal and electric demand. A reversible HP/ORC Carnot battery is integrated with the system to improve the flexible use of the renewable production and the thermal capacity of the DH substation. The electric grid is considered to satisfy the residual electric demand. An on-site thermal power source is included to improve the CB performance.

2.1. The energy system

This subsection describes the integrated energy system and provides a focus on the advantage of coupling the CB with the DH substation.

2.1.1. The integrated energy system

The integrated energy system considered in this study and the relationships among the subsystems are shown in Fig. 2 and briefly described below (the components in the figure are numbered according to the list). The main elements are:

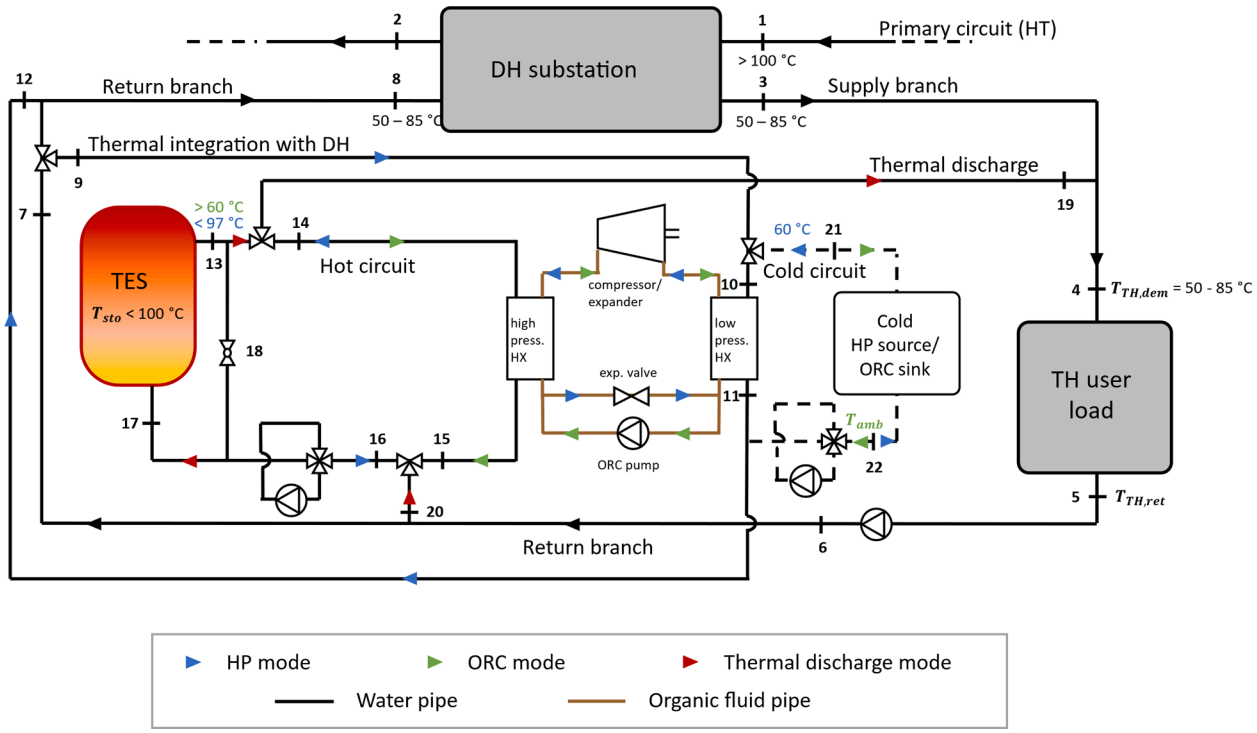

Fig. 4. Hydraulic circuit layout connecting the CB, the DH substation, and the thermal user.

1. An on-site electric power user and an on-site thermal power user, generating the demand temporal profiles, which must be covered by the generation and storage system in the study.
2. An on-site solar PV electric power generation plant (renewable energy source). The PV electricity production depends on the availability of solar irradiance at each timestep, and it can be compared with the electricity demand. The exceeding PV production can be sold to the grid or stored in the CB. In the latter case, the stored energy will be reconverted into power when a deficit in the renewable production occurs, and when the electricity price is high.
3. The electric grid, to which it is possible to sell the electricity surplus produced by the PV plant. The electric grid can be also used to fulfil the electric demand and to produce thermal power through the HP to satisfy the thermal demand.
4. The CB, composed of a reversible HP/ORC prototype and a Thermal Energy Storage (TES). The CB can be charged (HP mode) exploiting the PV power surplus or electricity from the grid to run the compressor. The CB can be discharged (ORC mode) to cover the electric user demand. The CB TES can be also discharged to cover the peaks in the thermal demand (thermal discharge), by directly using the stored thermal energy. The electricity production through the ORC may also occur in case of renewable production in surplus: in this case, the electrical production is sold to the grid.
5. An on-site thermal power source, which can consist of (i) a free waste-heat source or, (ii) a low-temperature DH line, used to feed the CB heat pump with a smaller temperature lift, thus obtaining a higher Coefficient Of Performance (COP). In the case of a free waste-heat source, the input thermal energy can be considered completely free in economic terms. In the second case, the input thermal power represents an economic cost for the CB.
6. The DH substation, primarily used to cover the thermal power demand. The DH entirely satisfies the thermal demand until it is lower than the substation size; when the demand overcomes the substation thermal output, the surplus is satisfied using the TES of the CB.

2.1.2. *Carnot battery – District heating coupling*

The coupling of a Carnot battery and a DH substation introduces more flexibility even on the thermal side (thermal demand/production). Part of the thermal energy stored in the CB storage may be used to satisfy the peaks occurring in the thermal power demand, allowing a downsizing of the DH substation, with a considerable reduction of the investment cost. As shown in Fig. 3, the thermal power demand profile (in red) presents a daily peak in the morning. In the absence of the CB, the thermal power provided by DH (in yellow) should cover the entire thermal demand at each instant of the day. In this case, the DH size should be at least as large as the highest thermal demand peak. On the contrary, the CB allows to fulfil the demand overshoot by the thermal power available in the CB TES (in orange), allowing a reduction of the DH size. The available thermal power that can be delivered by the TES (the maximum power that the storage could provide to the user at each time step) oscillates according to the thermal user's temperature level. The storage is recharged through the HP when renewable electric power from the PV (in blue) is available.

Furthermore, in some conditions, it could happen that the thermal energy available in the storage is not sufficient to cover the thermal demand peak, and, at the same time, the renewable production is not in surplus. In these cases, it could be economically convenient to buy electricity from the grid and satisfy the thermal demand peak through the HP, instead of increasing the size of the DH substation. However, this situation should not occur too often, otherwise, a larger DH substation would be more convenient. The size of the DH substation must be accurately designed to minimize the overall costs, namely considering both the investment (annual levelized) and the yearly operating costs.

The CB, the DH substation, and the thermal user are supposed to be connected according to the hydraulic circuit layout that is shown in Fig. 4. The black lines represent the water pipes, and the brown ones the reversible HP/ORC working fluid. The black arrows indicate the water flow direction when the DH satisfies the thermal demand, independently of the CB operation (path 3–4–5–6-7–8 in Fig. 4). The red arrows highlight the additional water streams in thermal discharge mode (path 13–19-4–5–6–20-16–17 in Fig. 4). The CB key streams and flow

directions in HP and ORC modes are described through respectively the blue and the green arrows. In HP mode, two reference cases are considered: i) "free waste heat" case, where the HP cold side is an external source (circuit represented by dashed lines in the figure, following the path 21–10–11–22 in Fig. 4); ii) "thermal integration with DH" case, where the HP cold side is the DH substation (path 3–4–5–6-7–9-10–11-12–8 in Fig. 4). In the 1st reference case, the HP is allowed to run during the thermal discharge mode, while it is not allowed in the 2nd reference case. The ORC is prevented from running during the thermal discharge mode (neither during HP mode). The constraints on the CB operation are further discussed in the next subsection, and some reference temperature values are provided to help the reader in the following parts of the paper.

2.2. The Carnot battery management strategy

The resolution of the problem is developed according to a rule-based strategy. The aim of investigating the influence of key design parameters and boundary conditions (namely PV and storage sizes, electricity cost, and environmental conditions) on the technical and economic performance requires an accurate model of the system, and the possibility of including numerous details without exponentially increasing the computational time. Detailed thermodynamic models require high computational effort, therefore, for the sake of modelling accuracy, the control strategy is "penalized" in its optimization, and thus it is based on a rule-scheduling approach. Thus, the proposed method allows to obtain a sub-optimum solution. The more the empirical rules adapt to a particular application the closer the solution will be to the optimal, but the less the same rules and the same strategy will be applicable to a different case study. The specific nature of the rule-based approach requires some changes in the scheduling strategy to be transferred to a different application.

The minimization of the costs drives the Carnot battery management strategy. In the following paragraphs, the physical problem and the control algorithm are described. The Carnot battery management strategy is fully implemented in MATLAB environment.

2.2.1. Problem description

The Carnot battery management strategy is called to decide the HP/ORC instantaneous load at each time step, to maximize the economic benefit provided by the integration of the CB in the entire system. The objective function (Eq. (1)) is the annual gain between two scenarios, i.e., with and without the Carnot battery intervention in the integrated system.

$$\Delta gain = R_1 + R_2 + R_3 + R_4 - C_1 - C_2(-C_3) \tag{1}$$

The gain is equal to the sum of four revenues, indicated with the letter R, minus two cost contributions (three in case the HP cold source is the DH instead of free waste heat), indicated with the letter C.

The first two positive terms (R_1 and R_2), calculated at each time step, are associated with the gain obtained by respectively the surplus sale ($E_{ORC,surplus}$) and the self-consumption ($E_{ORC,selfcons}$) of the ORC energy production:

$$R_1 = E_{ORC,surplus} \bullet C_{el,sale} \tag{2}$$

$$R_2 = E_{ORC,selfcons} \bullet C_{el,pur} \tag{3}$$

The surplus sale energy revenue, R_1, is proportional to the specific cost for the electricity sold to the grid ($C_{el,sale}$), as that electricity production is directly sold to the grid. While the self-consumption gain, R_2, is calculated as the cost saved by producing electricity for self-consumption, instead of buying it from the grid. Thus, the ORC production for self-consumption ($E_{ORC,selfcons}$) is multiplied by the purchasing electricity specific cost ($C_{el,pur}$), because, in case of absence of the ORC, that electricity would be purchased from the grid at the purchasing electricity cost.

The other two positive terms (R_3 and R_4) derive from the advantage of covering part of the thermal demand with the Carnot battery. The first one is related to the reduction of the investment cost when downsizing the DH substation, while the second is due to the thermal energy provided to the thermal user by the CB (Q_{CB2dem}), and saved from the DH (operating costs):

$$R_3 = \Delta size_{sub} \bullet C_{DH,fee}/lifetime \tag{4}$$

$$R_4 = Q_{CB2dem} \bullet C_{Q,DH} \tag{5}$$

The R_3 term represents the avoided levelized investment cost of the DH substation and it is proportional to: (i) the difference ($\Delta size_{sub}$) between the original and the new substation size (the original size is considered equal to the maximum thermal demand peak to be covered by the external thermal energy source), and (ii) the specific investment cost of the DH substation ($C_{DH,fee}$ in €/kW). The terms R_4 is proportional to the specific cost of heat purchased from the DH ($C_{Q,DH}$), because in the case without the CB the thermal energy contribution Q_{CB2dem} should be provided by the DH.

The cost contribution terms (C_1 and C_2), calculated at each time step, are associated with the HP electric consumption:

$$C_1 = E_{HP,ren} \bullet C_{el,sale} \tag{6}$$

$$C_2 = E_{HP,grid} \bullet C_{el,pur} \tag{7}$$

The cost C_1 derives from the renewable energy production ($E_{HP,ren}$) not sold to the grid, but used to feed the HP. Therefore, C_1 is proportional to the electricity sell price ($C_{el,sale}$) because, in the case without the CB, the electricity contribution $E_{HP,ren}$ would be sold to the grid. The cost C_2 is proportional to the specific purchase cost ($C_{el,pur}$) of the electricity used for the HP and purchased from the grid ($E_{HP,grid}$).

In case the thermal energy at the HP evaporator is provided by the DH (Q_{DH2HP}), one additional cost term C_3 is considered:

$$C_3 = Q_{DH2HP} \bullet C_{Q,DH} \tag{8}$$

The term C_3 is proportional to the specific purchase cost of heat from the DH ($C_{Q,DH}$).

The production of electricity for self-consumption allows for a downsizing of the electrical substation, but the different order of magnitude between the ORC electrical production and the electric demand makes it negligible, so it is not included in the objective function for this application case.

The maximization of the economic benefit, namely the economic gain $\Delta gain$, is performed through the optimization of three time-dependent variables at each time step. These variables are the HP/ORC electric power input/output, $\dot{W}_{HP}$ and $\dot{W}_{ORC}$, and the thermal power demand covered by the CB, $\dot{Q}_{CB2dem}$. The integrals of $\dot{W}_{HP}$, $\dot{W}_{ORC}$ and $\dot{Q}_{CB2dem}$ over the considered time period (a year) provide the energy terms ($E_{HP,ren}$, $E_{HP,grid}$, $E_{ORC,surplus}$, $E_{ORC,selfcons}$ and Q_{CB2dem}) that appear in the objective function (Eq. (1)). Therefore, $\dot{W}_{HP}$, $\dot{W}_{ORC}$, and $\dot{Q}_{CB2dem}$ are regulated so that to maximize the objective function $\Delta gain$.

The instantaneous constraints of the problem involve the HP/ORC operating limits (Eq. (9) and (10)), namely the system maximum load ($\dot{W}_{max}$), which depends on the storage temperature ($T_{sto}(t)$), and the minimum technical load ($\dot{W}_{min}$), otherwise, the reversible HP/ORC is not called to work. An additional constraint concerns the impossibility of the reversible CB working in ORC and HP mode simultaneously. The thermal power demand covered by the CB, $\dot{Q}_{CB2dem}$, is bounded by the minimum value between the storage available thermal power, $\dot{Q}_{CB,ava}$ (depending on the temperature profile in the storage and the thermal user temperature level), and the thermal user power demand, $\dot{Q}_{dem}$ (Eq. (11)).

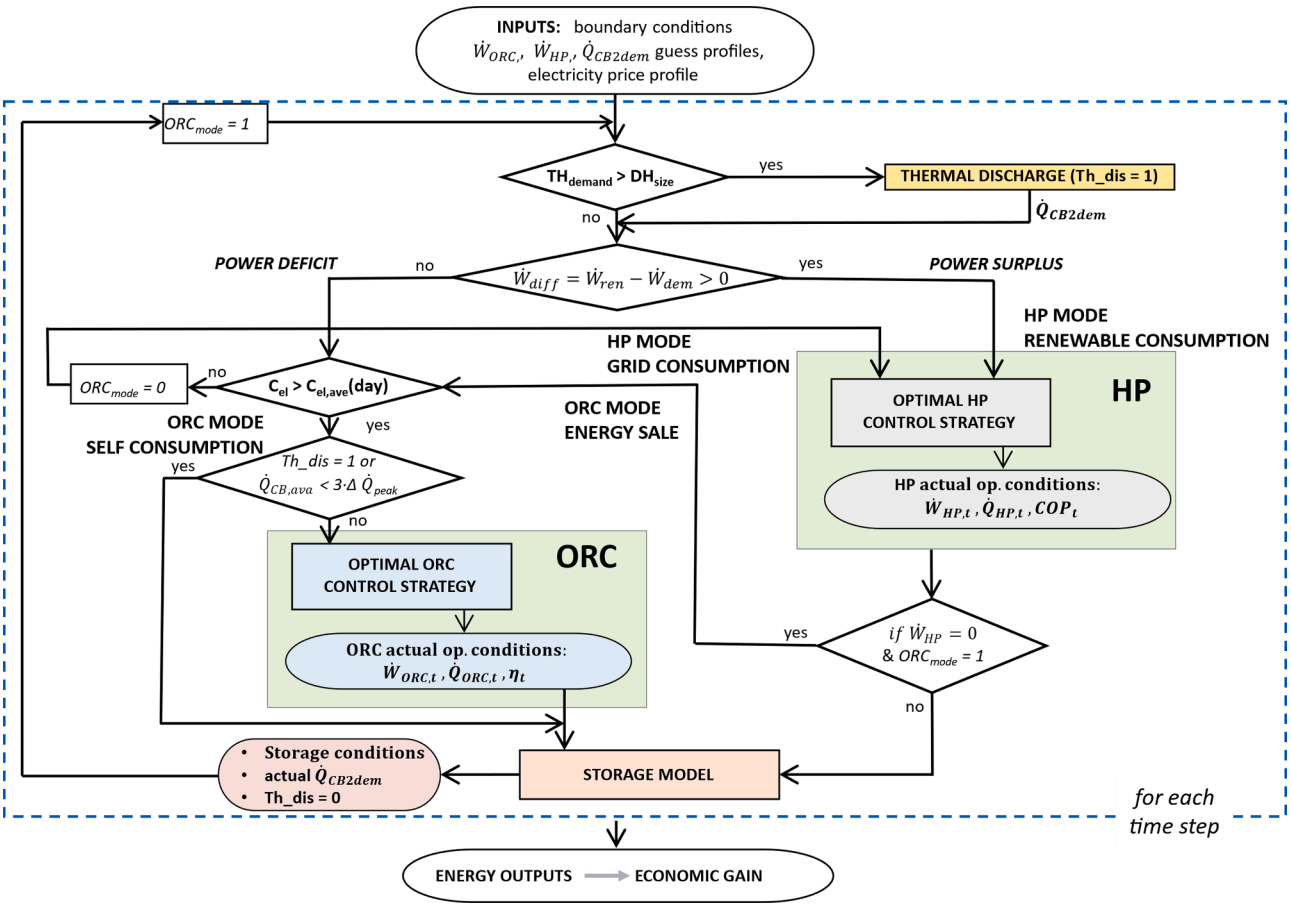

Fig. 5. The thermally-integrated CB control procedure flowchart.

$$\dot{W}_{HP}(t) = 0 \; or \; \in \left[\dot{W}_{min}, \dot{W}_{max}(T_{sto}(t))\right] \tag{9}$$

$$\dot{W}_{ORC}(t) = 0 \; or \; \in \left[\dot{W}_{min}, \dot{W}_{max}(T_{sto}(t))\right] \tag{10}$$

$$\dot{Q}_{CB2dem}(t) \in [0, min(\dot{Q}_{CB,ava}(T_{sto}(t), t), \dot{Q}_{dem}(t))] \tag{11}$$

in which $\dot{Q}_{CB,ava}$ is time-dependent and calculated as in Eq. (12):

$$\dot{Q}_{CB,ava}(t) = \frac{M_{sto} \bullet c_p \bullet (T_{sto}(t) - T_{TH,dem}(t))}{\Delta t} \tag{12}$$

where M_{sto} is the secondary fluid mass in the storage, c_p is the fluid specific heat at constant pressure, $T_{TH,dem}$ is the thermal user temperature level, and Δt is the time step (15 min in this study to comply with the system inertia).

Additional operating constraints of the HP/ORC systems are included as indicated by Eq. (13) and Eq. (14). The HP is not allowed to work if the storage temperature is higher than the maximum operating temperature ($T_{op,max}$), while the ORC is prevented to run if the storage temperature is lower than the minimum operating temperature for the ORC ($T_{ORC,min}$).

$$\dot{W}_{HP}(t) > 0 \; if \; T_{sto}(t) < T_{op,max}(t) \tag{13}$$

$$\dot{W}_{ORC}(t) > 0 \; if \; T_{sto}(t) > T_{ORC,min}(t) \tag{14}$$

2.2.2. The Carnot battery control logic numerical procedure

The resolution of the problem is executed by iteratively running the routine shown in Fig. 5, and reducing in each iteration the DH substation size level. Until the CB manages to cover all the thermal demand peaks, the DH substation size is reduced in each iteration. When the CB is no longer able to satisfy all the thermal demand peaks, the process is concluded, and the DH minimum substation size is defined. As shown later in the results, the downsizing of the DH substation provides most of the revenues due to the CB intervention. The reasons lie in the strong variation of the thermal demand profile, which presents daily high and narrow peaks. Through the TES, even with a small volume, it is possible to cover these peaks allowing for a considerable reduction of the DH substation size, and thus of the investment cost.

Once the DH substation size has been identified, the routine shown in Fig. 5 is run one more time to finally evaluate the economic benefit of adding the CB to the integrated system. The algorithm solves the problem by trying to maximize the annual gain, deciding to turn on/off the Carnot battery and/or switch between HP and ORC modes at each time step (15 min), according to the user demand profiles and the boundary conditions. Therefore, starting from a first attempt solution, the Carnot battery operation is simulated time step by time step, according to the detailed rule-based routine, shown in the flowchart in Fig. 5, and described below.

In the control strategy, priority is given to the thermal discharge, i.e., to the possibility of covering the thermal demand peaks with the thermal energy available in the storage. Thus, if the thermal demand is greater than the DH substation size, it means that there is a peak which should be covered by the CB stored thermal energy. Therefore, the DH covers a part of the thermal demand equal to its maximum capacity (which is equal to the substation size), while the rest of the thermal demand is covered by the thermal power available in the CB TES. This CB operating mode is named "Thermal discharge" ($Th_{dis} = 1$).

Then, the instantaneous PV electric power production is compared with the actual demand. If the electric demand is not entirely covered by the renewable production, it is the case of power deficit. So, the surplus in the demand must be covered through the ORC electric production or/

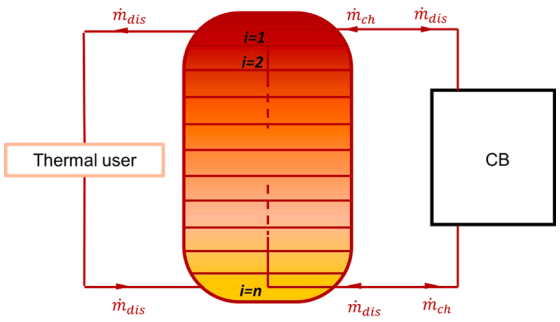

Fig. 6. Sensible TES discretization.

and electricity purchased from the grid. The convenience of running or not the CB, and if in ORC or HP mode, is assessed using the following rules:

First, the routine checks the instantaneous electricity price and compares it to the average electricity price of the current day (in Fig. 5, this check is represented by $C_{el} > C_{el,ave}(day)$). The daily average electricity price is simply calculated as the arithmetic mean of the values assumed by the electricity price within the day in which the current time step is included. If the instantaneous price is higher than the average, it can be more convenient to run the ORC to minimize the electricity that must be purchased from the grid, and thus to minimize the associated cost. If the electricity price is low, it would be better to buy the whole needed electricity and store the thermal energy to convert it when the grid electricity price is higher, or for the thermal discharge. In this case, since the electricity price is low, it can be convenient to buy electricity from the grid to charge the storage through the HP. Therefore, if the HP operating limits (Eq. (9)) are respected and the storage is not fully charged (Eq. (13)), then the HP is run according to its "optimal control strategy" (see next subsection), i.e., according to the operating conditions which maximize the HP COP.

If the electricity price is high (and so it could be convenient to run the ORC), the algorithm checks if during the current time step the thermal discharge is occurring (in Fig. 5, this check is represented by $Th_{dis} = 1$). If it occurs, the ORC is prevented from running, to avoid a further discharge of the storage with the risk of not covering the whole thermal demand peak. In other words, it is prevented the TES discharge through the ORC, to the detriment of the thermal demand peak shaving.

Before discharging the storage with the ORC, the algorithm checks also if the storage available thermal power is enough to cover the next three days' thermal demand peaks (in Fig. 5, this check is represented by $\dot{Q}_{CB,ava} < 3 \bullet \Delta\dot{Q}_{peak}$). This is a heuristic rule tuned by trial and error to reach a compromise to avoid buying too much electricity to satisfy the thermal demand peaks in the following days, in case of extended absence of the RES availability.

If these three rules and the ORC operating limits (Eq. (10) and Eq. (14)) are respected, then the ORC is run according to its "optimal control strategy" (see next subsection), i.e., according to the operating conditions which maximize the ORC efficiency, discharging the TES.

If the renewable production overcomes the electric demand, it is the case of power surplus. Therefore, if the HP operating limits (Eq. (9)) are respected and the storage is not full (Eq. (13)), then the HP is run according to its "optimal control strategy", absorbing part or the entire renewable electricity production in surplus, to charge the TES.

In case of power surplus and if the HP is not called to work ($\dot{W}_{HP} = 0$, because the storage is fully charged or the HP operating limits are not respected), the algorithm tests the possibility of running the ORC to produce a power surplus to sell to the grid. Again, before letting the ORC run, the algorithm checks i) the instantaneous electricity price, compared to the average price of that day, ii) the thermal discharge occurrence, and iii) the storage available thermal power at the current time step and to cover the next three days thermal demand peaks.

Eventually, the energy balance on the TES provides the updated conditions of the storage in terms of temperature profile and availability of thermal energy. A detailed description of the storage model block is provided in the next subsection. Furthermore, the boundary conditions are assumed as constant over the time step interval, so the HP/ORC system operation varies with time, but it is assumed to work in "quasi-steady state" operation during the time step interval.

2.3. Components modelling

This subsection briefly describes and provides some references for the modelling of the CB main components.

2.3.1. Reversible heat pump/organic Rankine cycle system

The HP/ORC operation and performance are determined through lookup tables, representing the system performance maps, which allow the identification of the maximum efficiency operation under imposed boundary conditions. Considering the available temperature in the storage, the temperature of the cold source/sink and the electric power availability/demand, the lookup tables provide the HP/ORC operating conditions that maximize the COP/efficiency. The HP/ORC operating conditions are provided in terms of effective electric power absorption/production, thermal power production/absorption, working fluid mass flow rate, and secondary fluids temperature glides (i.e., the secondary fluid temperature difference between heat exchangers inlet and outlet).

The used lookup tables are obtained by simulating the reference HP/ORC system in a wide range of operating conditions using a detailed off-design model based on a semi-empirical approach, in line with the off-design method modelling of micro-ORCs presented in [38] and reproduced and validated for another analysis in [39]. More in detail, the heat exchangers are modelled according to the moving boundaries method [40], the scroll compressor/expander is modelled according to the lumped parameter approach originally proposed by Lemort [41], the ORC pump is modelled according to [42], and the HP expansion valve is simply modelled as an isenthalpic expansion. A detailed description of the HP and ORC components modelling and the HP/ORC "optimal control strategy" is provided in section 4 in [23]. The HP/ORC model is calibrated and validated on the reversible prototype installed at the Thermodynamics Laboratory of the University of Liège (for the sake of brevity, the interested reader is invited to consult the dedicated experimental work [43]). The performance of the reversible HP/ORC model is evaluated in Chapter 4 of the PhD Thesis [38], in which the mean average percentage error of the global model is assessed to be lower than 2.5 %. The size of the system is rescaled to 10 kWe, considering the same efficiencies for the same boundary conditions, to meet the size of the new prototype that is being built at the University of Liège.

2.3.2. Sensible thermal energy storage

As a main component of the CB system, the sensible thermal energy storage has been modelled as a one-dimensional stratified water thermal energy storage tank. According to this approach, the tank is a vertical axis cylinder in which the water temperature varies only along the vertical direction, while the radial gradient is null. Thus, the storage volume is vertically discretized into a number n of equal-volume layers (Fig. 6), and inside each layer, the temperature is assumed as uniform [44]. The thermodynamic properties are allowed to vary between layers but not within a single layer, in accordance with the isothermal mixing zone methodology. Each layer is allowed to exchange energy with the adjacent layers through convection and diffusion, and with the tank wall through conduction. The energy conservation equation, applied to each layer, derives a system of n ordinary differential equations (Eq. (15)) [45].

$$\frac{M_{sto_i} \bullet c_p \bullet (T_i(t) - T_i(t-1))}{\Delta t} = \dot{m}_{ch} \bullet c_p \bullet (T_{i-1}(t) - T_i(t)) + \dot{m}_{dis} \bullet c_p \bullet (T_{i+1}(t) - T_i(t))$$

Table 1
Hypothesis and simulation parameters.

Reversible HP/ORC	Nominal Power (kW)	10
	Max op. Temperature (°C)	97
	ORC min op. Temperature (°C)	60
	ORC cold sink Temperature (°C)	T_{amb}
	HP cold sink (free waste heat) Temperature (°C)	60
TES	Volume (m^3)	10
	Aspect ratio (-)	6
	N° of Mixing Zones (-)	20
	Wall Thermal Resistance (m^2· K/W)	10
	Initial Temperature (°C)	95
	Max Temperature (°C)	100
PV Solar Panels	Area (m^2)	2000
	Efficiency (%)	25
DH	Min Temperature (°C)	50
	Max Temperature (°C)	85
Cost parameters	HP/ORC specific cost (€/kW)	2000
	Storage cost (€)	Eq. (8)
	Lifetime (years)	30
	Discount rate (-)	0.04
	DH fee (€/kW)	631
	Thermal energy price (€/kWh)	0.07

$$+\alpha \bullet M_{sto_i} \bullet c_p \bullet \frac{(T_{i+1}(t) + T_{i-1}(t) - 2T_i(t))}{\Delta x^2} - U \bullet A_i \bullet (T_i(t) - T_{amb}) \quad (15)$$

The left side of Eq. (15) shows the variation of the thermal energy in the i-th layer during time. M_{sto_i} is the fluid mass in the layer, c_p is the fluid specific heat at constant pressure, $T_i(t)$ is the temperature in the layer at the current time step and $T_i(t-1)$ is the temperature at the previous time step, Δt is the time step.

The right side of Eq. (15) presents all the contributions to the heat transfer occurring from one node to another and to the ambient. The first two terms represent the convection contributions occurring in the i-th layer, respectively during the charging and the discharging phases (see Fig. 6). The first term refers to the charging phase, when the fluid is forced to circulate from the top to the bottom of the tank, with a mass flow rate $\dot{m}_{ch}$. The second term occurs during the discharging phase, when the fluid is forced to circulate from the bottom to the top, with a mass flow rate $\dot{m}_{dis}$. The third term at the right side considers the diffusion occurring between the i-th layer and each of its two neighbours. α is the diffusivity coefficient, in m^2/s, and Δx is the thickness of the layer. The last term is associated with the thermal power dissipated to the ambient by conduction through the tank wall (and convection/radiation with the ambient at the other surface of the tank), where U is the global heat exchange coefficient through the wall, A_i is the i-th layer wall surface, and T_{amb} is the ambient temperature.

The problem is solved numerically by adopting the upwind scheme [46], providing the temperature profile in the storage tank as a function of time.

In the Annex, the storage temperature profile is shown for general weeks in winter (Fig. A2) and in summer (Fig. A3). Each colour line represents the temperature profile of a particular layer in which the storage volume is discretized. In summertime, the storage temperature is allowed to significantly decrease because the stored thermal energy is not required to satisfy the thermal demand, thus the ORC is allowed to exploit the stored energy whenever the electricity price makes it convenient, and the technical conditions are matched. In wintertime, the priority is given to the thermal discharge, and the need to operate it at the temperatures required by the user significantly constraints the ORC operation, and thus the TES temperature variation.

2.4. Hypotheses and boundary conditions

This subsection presents all the hypotheses and the parameters adopted in this study, as detailed in Table 1.

2.4.1. User energy profiles

The user's energy profiles, namely the electric and the thermal demands, derive from data collected in a 2000 m^2 building, comprising laboratories and offices, at the University of Liège campus over a year. The electric and the thermal demands are mostly due to the lightening and the heating of the building. The user energy demand profiles are shown in Fig. 7 with the negative sign to highlight that they need to be compensated by the different involved subsystems (i.e., the PV panels, the grid, and the ORC for the electric demand; the DH substation and the CB storage for the thermal demand). The electric power is required during the full year, and it presents some peaks occurring during the working hours. The thermal demand is almost null during summer months, while in winter months it presents a high peak in the early morning of the working days.

2.4.2. Photovoltaic solar panels and district heating

A photovoltaic solar power plant, with a surface area equal to 2000 m^2, represents the renewable energy source. The solar panels surface is considered as oriented with the optimal angulation for Liège coordinates (40-degree slope and −5-degree Azimuth), and a constant efficiency equal to 25 % is assumed for the PV plant. The renewable production (Fig. 7) is simulated considering the solar irradiance profile that occurred in Liège in 2020 [47]. In the present work, for the sake of simplicity and since the focus is the economic convenience of integrating the Carnot battery into a more complex system, the PV power plant has not been modelled in detail. Indeed, the renewable electricity production varies directly with the irradiance profile, of a constant value equal to the product between the PV efficiency and the surface area.

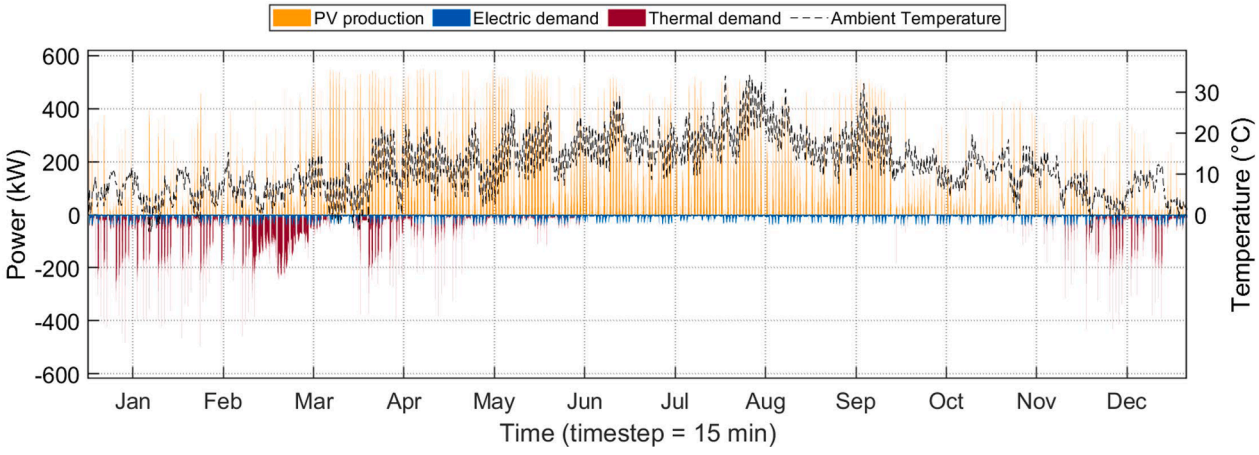

Fig. 7. Renewable production, ambient temperature, and user energy profiles.

Therefore, an average reduction of the PV efficiency can be perfectly compensated with an increase in the surface area. The hypothesis of PV constant efficiency is applied in this first analysis. A variable PV modules efficiency would modify the instantaneous electricity production compared to the case with the constant efficiency hypothesis. However, a reduction of the PV surface area does not significantly affect the overall economic gain (it will be shown in the 'Results and Discussion' section), but only the cost distribution between the electricity bought from the grid and the renewable electricity consumed by the HP. In any case, this simplification could be removed in a future study, implementing a model of the PV power plant, to assess the impact of variable efficiency on the yearly distribution of the operating costs.

An interesting alternative is to consider photovoltaic thermal panels, instead of the base PV technology. In this case, the panels efficiency is typically high, and the renewable energy source provides both the electricity to satisfy the user's electric demand, and a thermal booster for the HP performance improvement. The application in DH of PV thermal panels in combination with HP is being extensively investigated [48], since the PV thermal alone does not reach the temperature levels required by conventional DH networks like the one already implemented in the reference campus. For example, Obalanlege et al. [49] analyse an integrated system composed of a PV thermal panel, a water tank and a HP for residential space heating and electricity provision. Mi et al. [50] investigate the economic convenience of integrating a PV thermal power plant with a HP to feed a DH network in Dalian, China, and they demonstrate that the proposed system could bring significant improvements in the system efficiency and costs. They show that the PV thermal HP requires only 30 % of the equivalent consumption of an air source heat pump and 12 % of an electric boiler. Therefore, PV thermal technology is an interesting upgrading of base PV technology for tertiary sector applications addressing both thermal and electrical energy demands. The adoption of a CB as energy storage in such a context is the most reasonable. Indeed, even if the use of Li-ion batteries would ensure higher roundtrip efficiency and energy density, and lower long-term costs, they present higher medium costs and sustainability issues for manufacturing and recycling. Parra et al., in their techno-economic comparison [51] among the use of Li-ion batteries, lead-acid batteries and hot water storage tanks for PV storage systems, find that the hot water tanks are the most economical option in the UK. Furthermore, also according to Pakere et al. [52], it is economically convenient to convert excess electricity into heat when the market electricity price is low. Eventually, adopting a different electric energy storage system in the reference university building application, it would be necessary to also include another thermal production system (i.e., a solar thermal collector) to support the DH during the peaks in the thermal demand.

The district heating substation that covers the reference building thermal demand works at temperatures between 50 and 85 °C, which are lower than the campus DH primary circuit temperatures (>100 °C), as also shown in Fig. 4. Therefore, the thermal user temperature level is constrained below 85 °C. The DH supply (upstream the thermal user) and return (downstream the thermal user) branches temperature profiles adopted derive from the data collected for the reference university campus building (see Fig. A1 in the Annex).

2.4.3. Carnot battery system and the free waste heat

The reversible HP/ORC system has a nominal electrical power of 10 kWe, and it works with HFO-1233zd(E), a high-performing, non-flammable, ultra-low GWP (less than1 [53]) refrigerant. The 10 kWe-sized test bench that is currently being installed at the Thermodynamics Laboratory of the University of Liège is considered as reference. The hot ORC source/HP sink temperature level varies in the range between 60 and 97 °C. The upper limit is set to avoid reaching temperatures much higher than the DH substation operating temperatures (50–85 °C) and the thermal user demand temperature, which would unnecessarily decrease the HP performance. The lower bound corresponds to the minimum hot source level of temperature at which the ORC is allowed to work, to avoid reaching extremely low conversion efficiency. Regarding the cold ORC sink/HP source temperature, the ORC condenser operates with water at the external ambient temperature (the ambient temperature profile in Liège in 2020 [47] is considered, shown in Fig. 7). The HP works with a lower temperature lift (temperature difference between the hot sink and the cold source) to increase its performance, resulting in a thermally integrated CB. The evaporator in HP mode works with thermal energy available at 60 °C and coming from a free waste source or from the DH substation (both cases are analysed and discussed in the results section). The considered free waste heat source may have several origins in a university campus. One of the most abundant waste heat sources is the thermal energy released by the data centers, widely present in the reference campus. Data centers work almost uninterruptedly, and the liquid cooling allows to reach return hot water temperatures of 50–60 °C [54], in line with the requirements for the reference application.

2.4.4. The thermal energy storage reservoir

The storage is a water cylindrical tank of 10 m^3 and with an aspect ratio of 6. The volume is discretized into 20 layers, as a good compromise between accuracy in the TES temperature profile and computational effort. Indeed, it has been observed that the temperature profiles of the layers do not significantly change with a number of layers of 20 or greater, while the computational time significantly increases (see Fig. A4 in the Annex). The wall thermal resistance is set at 10 $m^2 \cdot$ K/W, according to [55]. The maximum temperature is limited to 97 °C, in line with the constraint imposed on the reversible HP/ORC system operations, while the initial temperature is set to 95 °C.

2.4.5. Cost correlations and electricity price profiles

To perform the economic analysis, an estimation of the investment costs for the reversible HP/ORC system and the storage tank has been assessed. For the reversible HP/ORC plant, a single specific cost of 2000 €/kWe has been considered assuming a size of 10 kWe in HP mode. The HP/ORC investment cost hypothesis is high compared to the estimated costs of ORC projects in past studies [56], although the price range for heat pump and Rankine cycle technologies assumed in a recent study on CB [13] is in line with the current investigation. The assumed costs are in view of an industrial production, rather than costs of a prototype, considering rescaling the system to a larger size. For this purpose, a sensitivity analysis has been performed by varying the reversible HP/ORC specific cost for the investment.

The storage investment cost is calculated through Eq. (16) [57], where V is the TES volume in m^3:

$$I_{TES} = \log(V) - 0.002745 \bullet V^2 + 902.6 \bullet V + 7061 \quad (16)$$

Moreover, the lifetime of the CB is assumed equal to 30 years and the discount rate is set at 0.04 [58].

The DH substation specific investment cost ($C_{DH,fee}$) is considered equal to 631 €/kWth since the DH substation size is in the range between 200 and 1200 kW [59]. This value, multiplied by the difference between the original DH substation size and the new one ($\Delta size_{sub}$), provides the economic saving which can be obtained in the investment cost of the DH substation. Furthermore, the purchase price of the DH thermal energy has been set constant and equal to 0.07 €/kWh, as provided by the grid regulator [59].

The hourly spot market profile in Belgium in 2021 [60] is adopted as the reference electricity price profile. In the first part of that year the daily average prices were similar to the one occurring in the years before, while in the second part of the year, the price of the electricity increased to the average values that occurred in 2022. Therefore, the year 2021 for the electricity price profile has been chosen as a compromise between the previous years, in which the prices were lower, and 2022, in which the electricity price increased significantly. The considered electricity purchase price (C_{pur}) is increased of a value of 0.12

€/kWh ($\Delta price_{ref} = C_{pur} - C_{sale}$) compared to the electricity sale price (C_{sale}) (assumed equal to the spot market profile). These data are related to the reference case study, but a sensitivity analysis varying the electricity cost has been performed and discussed in the results section. The electricity price profiles for the year 2021 are shown in Fig. A5 in the Annex.

2.5. Performance indicators

To evaluate the techno-economic performance, resulting from the integration of a reversible HP/ORC Carnot battery with a DH substation and a PV power plant, some relevant energy and economic indicators are introduced in this study.

The performance indexes related to the CB operation are as follows:

The annual electric energy terms (in kWh) consumed by the HP (E_{HP}) and produced by the ORC (E_{ORC}), obtained as the sum of respectively the electric power consumption ($\dot{W}_{HP}$) occurring in HP mode operation and the electric power production ($\dot{W}_{ORC}$) occurring when the CB works in ORC mode:

$$E_{HP} = \sum \dot{W}_{HP} \bullet \frac{\Delta t}{3600} \tag{17}$$

$$E_{ORC} = \sum \dot{W}_{ORC} \bullet \frac{\Delta t}{3600} \tag{18}$$

The annual thermal energy terms (in kWh) produced by the HP (Q_{HP}) and absorbed by the ORC (Q_{ORC}) obtained as the sum of respectively the thermal power production ($\dot{Q}_{HP}$) in HP mode operation and the thermal power consumption ($\dot{Q}_{ORC}$) in ORC mode:

$$Q_{HP} = \sum \dot{Q}_{HP} \bullet \frac{\Delta t}{3600} \tag{19}$$

$$Q_{ORC} = \sum \dot{Q}_{ORC} \bullet \frac{\Delta t}{3600} \tag{20}$$

The average coefficient of performance (COP_{ave}) and the average efficiency (η_{ave}), defined respectively for the HP mode and for the ORC mode according to Eq. (21) and (22). They are obtained respectively as the ratio between the thermal energy produced by the HP (Q_{HP}) and the electric energy consumed by the HP (E_{HP}), and the ratio between the electric energy produced by the ORC (E_{ORC}) and the thermal energy absorbed by the ORC (Q_{ORC}):

$$COP_{ave} = \frac{Q_{HP}}{E_{HP}} \tag{21}$$

$$\eta_{ave} = \frac{E_{ORC}}{Q_{ORC}} \tag{22}$$

Since part of the thermal energy produced by the HP and stored in the TES is used to satisfy the thermal demand, an additional performance indicator is the thermal energy directly discharged to the thermal user (Q_{CB2dem}). The HP thermal energy consumption ($Q_{HP,DH}$) is also considered. This quantity gains importance especially if the HP cold source is not free waste heat, but thermal energy purchased from the DH, thus with an economic cost.

$$Q_{CB2dem} = \sum \dot{Q}_{CB2dem} \bullet \frac{\Delta t}{3600} \tag{23}$$

$$Q_{HP,DH} = \sum \dot{Q}_{HP,DH} \bullet \frac{\Delta t}{3600} \tag{24}$$

The CB running hours include the number of operating hours both in HP mode and in ORC mode.

The CB roundtrip efficiency (RTE), defined as the ratio between the electricity reconverted by the ORC (E_{ORC}) and the portion of electricity stored in the CB that will be returned by the ORC ($(Q_{HP} - Q_{CB2dem})/COP_{ave}$):

$$RTE = \frac{E_{ORC}}{(Q_{HP} - Q_{CB2dem})/COP_{ave}} \tag{25}$$

The effectiveness of integrating the CB with PV panels, to limit the mismatch between the electric power production and the user demand, is evaluated through the following indicators [61]:

The self-consumption rate (γ_{cons}), which is defined as the fraction of electric energy consumed by the user, including the HP consumption that has been covered by the renewable production, including the ORC reconverted electricity.

$$\gamma_{cons} = \frac{\sum \min\left(E_{cons}, E_{prod}\right)}{\sum E_{cons}} \tag{26}$$

The self-production rate (γ_{prod}), defined as the fraction of electric energy produced by the renewable production, including the ORC that has been consumed by the user and the HP.

$$\gamma_{prod} = \frac{\sum \min\left(E_{cons}, E_{prod}\right)}{\sum E_{prod}} \tag{27}$$

where E_{cons} is the sum of the electric demand and the HP electric consumption, and E_{prod} is the sum of the PV panels production and the ORC electric production. In the results section, γ_{cons} and γ_{prod} are compared to the case without the CB intervention.

Finally, the economic benefit of adding the CB to the integrated system, consisting of the PV power plant and the DH substation to satisfy the user thermal demand, is highlighted as follows:

The DH substation downsizing ($\Delta size_{sub}$), defined as the difference between the DH substation size without CB ($DHsize_{woCB}$) and with CB ($DHsize_{wCB}$) (Eq. (28)). It provides an economic benefit in terms of saving in the DH substation investment cost (ΔI_{DH}), proportional to the DH fee ($C_{DH,fee}$) (Eq. (29)):

$$\Delta size_{sub} = DHsize_{woCB} - DHsize_{wCB} \tag{28}$$

$$\Delta I_{DH} = \Delta size_{sub} \bullet C_{DH,fee}/lifetime \tag{29}$$

The annual differential economic gain, $\Delta gain$, (Eq. (1)) which is the difference between the economic benefit obtainable in the two scenarios, namely with and without the Carnot battery intervention in the integrated system.

The payback period (PB) [62] and the discounted payback period (DPB). They are evaluated by equalling the CB investment cost, namely the reversible HP/ORC investment cost ($I_{HP/ORC}$) and the storage investment cost (I_{TES}), to respectively the differential economic gain (Eq. (30)) and the actualized differential economic gain (Eq. (31)), in which the discount rate r is considered.

$$PB = \frac{I_{HP/ORC} + I_{TES}}{\Delta gain} \tag{30}$$

$$\sum_{t=1}^{DPB} \frac{\Delta gain}{(1+r)^t} = I_{HP/ORC} + I_{TES} \tag{31}$$

3. Results and discussion

Results are provided and compared for the two reference cases in terms of the HP cold source, namely the “free waste heat” (1st reference case) and the “thermal integration with DH” (2nd reference case). Moreover, the control optimization is highlighted, showing the results obtainable when changing some rules in the control flowchart, for the first case. Furthermore, sensitivity analysis varying the PV plant surface area, the storage volume, the electricity price profile, and the reversible HP/ORC investment cost is presented.

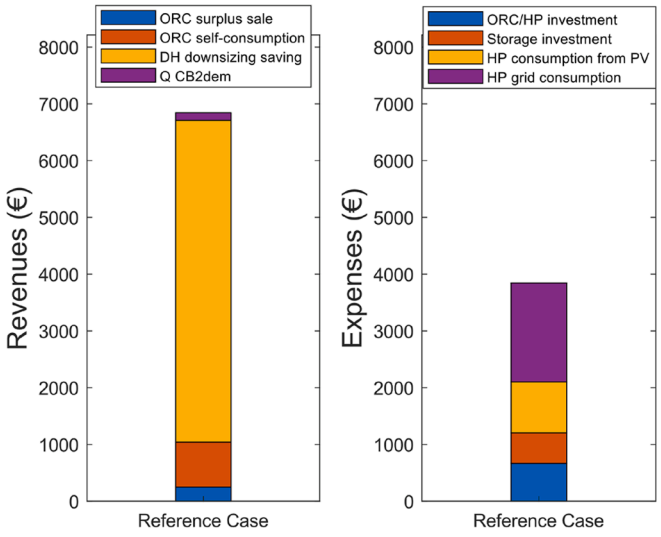

Fig. 8. Carnot battery annual revenues and expenses for the 1st reference case: R1 – ORC surplus sale, R2 – ORC self-consumption, R3 – DH downsizing saving, R4 – Q CB2dem, C1 – HP consumption from PV, C2 – HP grid consumption.

Table 2
Annual results for the 1 st reference case.

Mode	Charge - HP	Discharge - ORC	Thermal discharge
COP/efficiency (-)/(%)	4.84	8.42	–
Electrical energy (kWh)	16,300	5280	–
Thermal energy (kWh)	78,843	62,735	1943
Running hours (h)	1630	1506	28.5
Roundtrip efficiency,*RTE*(%)	33.2		–
DH downsizing, $\Delta size_{stub}$ (kW)	269.5 *(size without the CB intervention: 575.1)*		
Self-consumption rate, γ_{cons} (%)	44.3 *(41.8 without the CB intervention)*		
Self-production rate, γ_{prod} (%)	9.49 *(8.03 without the CB intervention)*		
PB (years)	8.59		
DPB (years)	10.2		

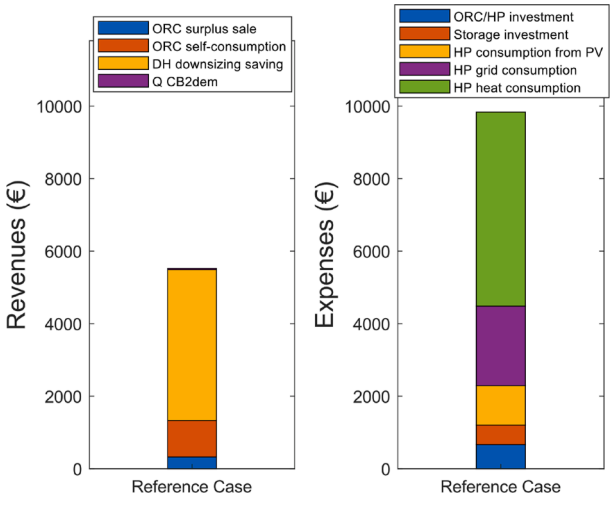

Fig. 9. Carnot battery annual revenues and expenses for the 2nd reference case: R1 – ORC surplus sale, R2 – ORC self-consumption, R3 – DH downsizing saving, R4 – Q CB2dem, C1 – HP consumption from PV, C2 – HP grid consumption, C3 – HP heat consumption.

Table 3
Annual results for the 2nd reference case.

Mode	Charge - HP	Discharge - ORC	Thermal discharge
COP/efficiency (-)/(%)	4.85	8.49	–
Electrical energy (kWh)	19,860	6701	–
Thermal energy (kWh)	96,294	78,919	510
Running hours (h)	1986	1849	12
Roundtrip efficiency,*RTE*(%)	33.9		–
DH downsizing, $\Delta size_{stub}$ (kW)	197.8		
Self-consumption rate, γ_{cons} (%)	44.8		
Self-production rate, γ_{prod} (%)	9.79		
PB (years)	–		
DPB (years)	–		

3.1. Reference cases results

The two reference cases differ for the HP cold source. Indeed, in the 1st case, the HP evaporator absorbs thermal energy from available free waste heat, while in the 2nd case, the thermal energy to the evaporator is provided by the DH return branch. The simulation results of the two reference cases are discussed and compared in the current section.

3.1.1. 1st reference case: Free waste heat as heat pump cold source

The additional revenues and expenses due to the integration of the Carnot battery with a PV power plant and a DH substation, to satisfy the reference thermal and electric user demands, are shown in Fig. 8. Most of the revenues are provided by the reduction of the DH substation size, which allows for significantly lower investment costs. Indeed, over 7000 € of yearly revenues, more than 5000 € are due to the downsizing of the DH substation. In contrast, the gain directly obtained with the CB thermal energy, covering the demand instead of buying it from the DH, is almost negligible. Therefore, the gain due to the CB intervention with the DH is nearly totally provided by the significant reduction of the DH investment costs, rather than the operating costs. The other revenues are due to the ORC production for self-consumption, to a greater extent, and a small part for selling to the grid. Concerning the expenses, they are associated with the CB investment cost and the HP electricity consumption, both from the grid and the PV production, which is not sold to the grid.

Table 2 shows the CB annual performance highlighting the contribution of the three different modes (HP mode, ORC mode, and thermal discharge mode). The HP charges the storage for about 1630 h during a year of operation, producing 78,843 kWh of thermal energy. The HP thermal production is mostly used as input for the ORC and reconverted into 5280 kWh of electricity. The ORC operates for about 1506 h with an average efficiency of 8.42 %. A small fraction of the stored heat (1943 kWh) is directly sent to the thermal user in pure thermal discharge mode, to cover the early morning thermal demand peaks. The thermal peak shaving effect (see also Fig. A6 in the Annex) allows for a downsizing of the DH substation. In particular, the $\Delta size_{stub}$ term is equal to 269.5 kW, corresponding to almost half of the peak demand 575.1 kW (size required to cover the entire thermal demand without the CB). Fig. A7 in the Annex shows the electric power profile in a general summer week, for comparison purpose. Concerning the electricity balance of the plant, about 44 % of the electricity demand is covered by the renewable production, and 9.5 % of the PV production is consumed by the user. Both the self-consumption rate and the self-production rate increase, in comparison with a scenario without the CB (41.8 % and 8.03 % respectively). This result shows that the CB operates as an electricity storage device, i.e., it limits the mismatch between the renewable production and the user consumption. Eventually, in this reference case, the calculated PB is equal to 8.5 years and the DPB is close to 10 years.

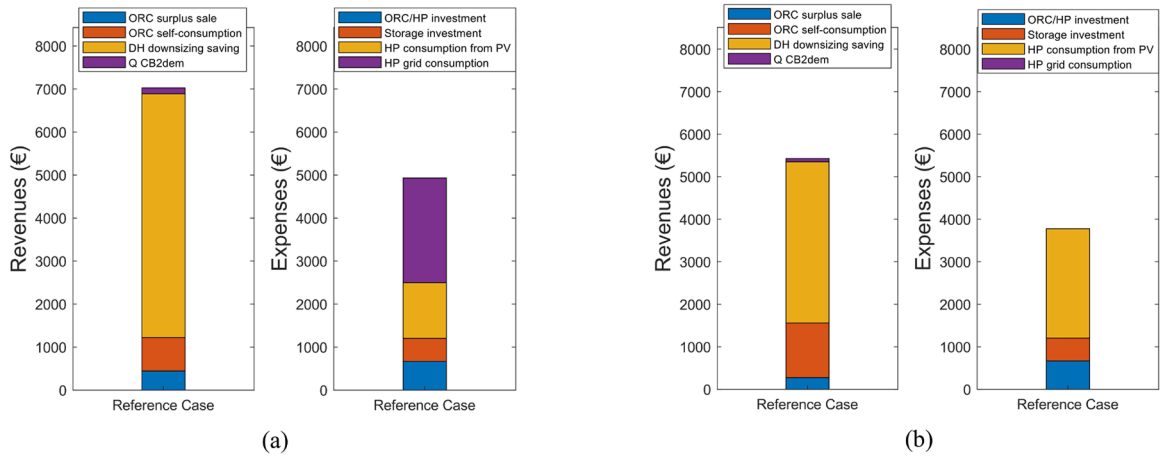

Fig. 10. Carnot battery annual revenues and expenses when removing (a) the electricity price constraint and (b) the possibility of feeding the HP with electricity from the grid.

Table 4
Results for the comparison of the CB annual economic performance when the control strategy is modified.

	Without electricity price constraint	Without the possibility of feeding the HP with electricity from the grid
DH downsizing, $\Delta size_{sub}$ (kW)	269.5	180.3
Self-consumption rate, γ_{cons} (%)	46.1	53.9
Self-production rate, γ_{prod} (%)	10.3	12.2
PB (years)	10.9	12.6
DPB (years)	13.9	17.0

3.1.2. 2nd reference case: District heating thermal energy as heat pump cold source

In the "thermal integration with DH" scenario, the CB economic benefit is also affected by the purchase cost of heat from the DH. As shown in Fig. 9 (b), the HP thermal energy consumption is responsible for the largest cost contribution, leading to a value of the expenses more than double of the costs term in the 1st case.

A decrease in the revenues also occurs because of a reduction in the DH substation downsizing. Since the CB absorbs thermal energy from the DH when operating in HP mode, the HP is not allowed to work when the thermal discharge mode occurs. The DH substation is already exploited at its nominal power, so it is not able to provide thermal energy to the HP. Therefore, the HP is not allowed to provide a booster to the TES when the thermal discharge occurs, preventing a further downsizing of the DH substation. Indeed, as reported in Table 3, the DH substation downsizing is only of 198 kW. However, a larger size of the DH substation requires the CB to cover only the highest peaks, therefore a larger amount of thermal energy is available during the rest of the day to run the ORC, whose production results increased in this 2nd case, rather than in the 1st case. To compensate for the increase of the ORC running hours, an increment of the HP working hours and consumption occurs.

According to the results of the analysis of the 2nd case, the integration of the CB with a DH substation when waste heat is not available, and absorbing thermal energy from the DH to run the HP, is not economically convenient (i.e., the expenses are larger than the revenues, under the considered boundary conditions). Therefore, this case is not further considered in the rest of the paper, but only the graphs with guidelines are shown in the Annex.

3.2. Effect of control optimization

This subsection aims to give evidence of the benefits added by the constraint on the electricity price and the HP grid consumption in the control strategy. A comparison of the annual economic performance when the CB is integrated with the reference system (1st case) is discussed.

Fig. 10(a) shows the annual revenues and expenses provided by the CB when the constraint on the electricity price ($C_{el} < C_{el.ave}(day)$) is removed (see Fig. 5). Letting the ORC discharge the storage as soon as possible, without waiting for a higher electricity price (within a day), slightly increases the ORC production because there are fewer constraints on the ORC operation. More in detail, the economic gain due to the production for self-consumption decreases, while the gain from the electricity sold by the ORC slightly increases (see Fig. 8 for comparison). Furthermore, the cost of the HP electricity increases significantly to compensate for the higher ORC production, and because electricity is purchased also when the price is high. The HP renewable electricity consumption increases because the removal of the electricity cost constraint lets both the HP and ORC work alternatively and more frequently. For this reason, the ORC production for selling increases. Eventually, the DH substation downsizing is not affected by this variation in the control algorithm. As a result, the removal of the electricity cost constraint reduces the economic benefit provided by the CB intervention, and thus increases its PB period, which is assessed to be about 11 years (Table 4).

To avoid the increase in the HP cost, the possibility of purchasing electricity from the grid to feed the HP may be removed. Fig. 10(b) shows the annual revenues and expenses provided by the CB when both the constraint on the electricity price and the possibility of feeding the HP with electricity from the grid (HP grid consumption) are removed. The DH substation downsizing significantly decreases (Table 4), thus the economic benefit associated with it is lower than in the reference case (Fig. 8). Reasons lie in the absence of the possibility to charge the storage and boost the thermal production of the CB, also when the solar radiation is too low or absent. Therefore, the CB can shave only a smaller part of the thermal demand peaks. Because of the larger size of the DH substation, less thermal energy is provided by the CB, and only the highest peaks are covered by the energy stored in the TES. As a result, a larger amount of thermal energy is available to run the ORC, whose production increases (Fig. 10(b)). Furthermore, the absence of the HP grid consumption reduces the overall HP consumption costs, but it increases the self-consumption of the electricity produced by PV panels. With this hypothesis in the control algorithm, the PB period results higher than 12 years.

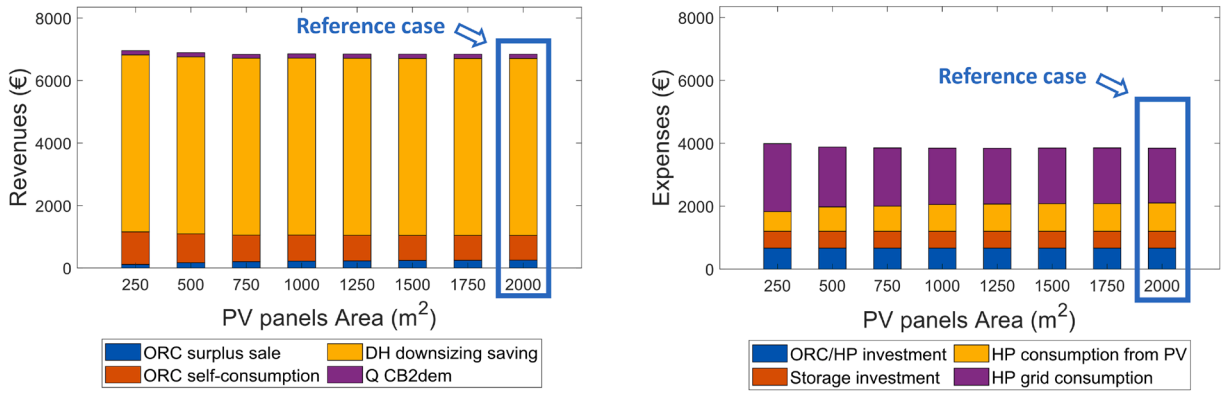

Fig. 11. Carnot battery annual revenues and expenses when varying the PV surface for the 1st reference case.

Table 5
Annual results when varying the PV surface for the 1st reference case.

PV surface (m^2)	250	500	750	1000	1250	1500	1750	2000
DH downsizing, $\Delta size_{sub}$ (kW)	269.5	269.5	269.5	269.5	269.5	269.5	269.5	269.5
Self-consumption rate, γ_{cons} (%)	30.9	36.9	39.7	41.3	42.4	43.2	43.8	44.4
Self-production rate, γ_{prod} (%)	50.2	30.8	22.3	17.5	14.4	12.3	10.7	9.49
PB (years)	8.64	8.56	8.57	8.57	8.57	8.59	8.60	8.59
DPB (years)	10.3	10.2	10.2	10.2	10.2	10.2	10.2	10.2

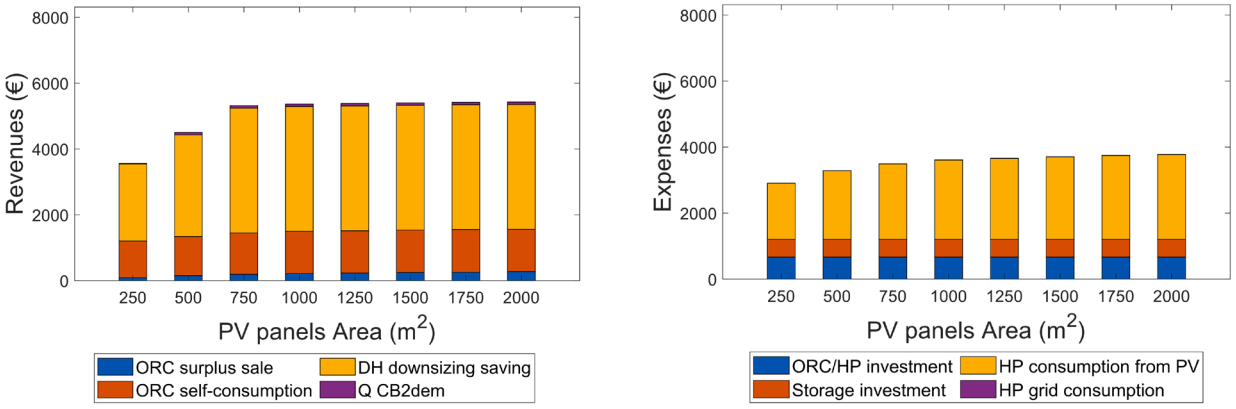

Fig. 12. Carnot battery annual revenues and expenses when varying the PV surface for the 1st reference case when removing the electricity price constraint and the possibility of feeding the HP with electricity from the grid.

Removing the constraint on the electricity price and the HP grid consumption, both the self-consumption and the self-production rates increase (Table 4), because of the larger exploitation of the renewable production by the HP.

As a conclusion of this analysis, despite the increase in the self-consumption, a decrease in the economic profit is observed when the instantaneous electricity price is not considered in the regulation strategy and the HP is prevented from absorbing electricity from the grid.

3.3. Effect of the photovoltaic panels surface

A parametric analysis varying the photovoltaic power plant surface area has been performed to analyse the system performance variation varying the renewable energy input. The analysis is shown for the 1st reference case (the 2nd is in the Annex), varying the PV panels area from 250 to 2000 m^2 with a step of 250 m^2. Smaller surfaces are not shown in the analysis because too small for the reference CB to provide an economic benefit. Larger surfaces have not been considered, since the aim is to try decreasing the PV area compared to the reference cases, and thus to reduce the PV investment cost.

Fig. 11 shows the annual revenues and expenses associated with the CB when varying the PV panels area, in the case in which free waste heat is available as the HP cold source. Both the revenues and the expenses are almost constant. Only in the case when the PV panels area is 250 m^2, the HP consumption is slightly higher than in the other cases. The increase of the PV surface results in a larger renewable production, which can be stored in the CB until the HP does not work at its full capacity. Indeed, in the first two cases with the smallest PV surface, the percentage of the HP renewable consumption over the whole HP consumption is lower than in the other cases, in which this value tends to flatten. More in detail, with a PV panels area of 250 m^2 the HP renewable consumption represents 22 % of the whole HP consumption, when the PV panels area is increased to 500 m^2 the HP renewable consumption rises to 29 %, for larger PV surfaces this ratio remains always between 31 and 34 %.

Furthermore, as shown in Table 5, the self-consumption rate increases with the PV surface, and the self-production rate decreases. The reason is due to the increase of the renewable production, which can

Table 6
Annual results when varying the PV surface for the 1st reference case when removing the electricity price constraint and he possibility of feeding the HP with electricity from the grid.

PV surface (m^2)	250	500	750	1000	1250	1500	1750	2000
DH downsizing, $\Delta size_{sub}$ (kW)	111.3	146.7	180.3	180.3	180.3	180.3	180.3	180.3
Self-consumption rate, γ_{cons} (%)	37.9	44.8	48.4	50.5	51.7	52.6	53.4	53.9
Self-production rate, γ_{prod} (%)	61.9	38.5	28.3	22.4	18.5	15.8	13.8	12.2
PB (years)	19.5	14.9	11.9	12.2	12.3	12.4	12.5	12.6
DPB (years)	35.2	21.7	15.6	16.1	16.4	16.6	16.8	17.0

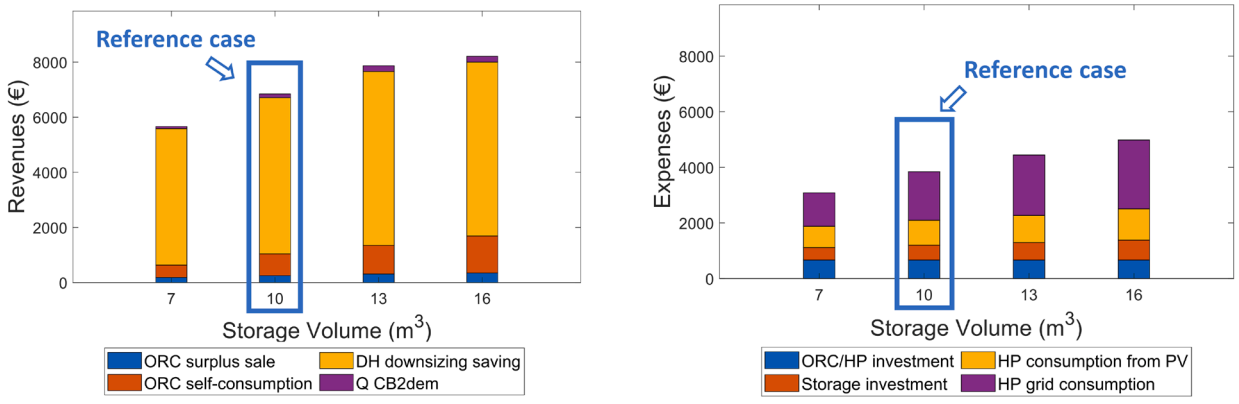

Fig. 13. Carnot battery annual revenues and expenses when varying the storage volume for the 1st reference case.

Table 7
Annual results when varying the storage volume for the 1st reference case.

Storage volume (m^3)	7	10	13	16
DH downsizing, $\Delta size_{sub}$ (kW)	235.5	269.5	300.0	300.0
Self-consumption rate, γ_{cons} (%)	43.7	44.4	44.7	45.6
Self-production rate, γ_{prod} (%)	9.12	9.49	9.71	10.1
PB (years)	9.04	8.59	8.22	9.01
DPB (years)	10.9	10.2	9.70	10.8

cover a larger part of the electric demand.

When removing the HP grid consumption, the DH substation downsizing is affected by the PV panels area reduction only for the two cases with the smallest surfaces (Fig. 12). In these two cases, the lower availability of renewable electricity prevents the HP from running at its full capacity to produce the required thermal energy to further downsize the DH substation. Both the HP consumption and the ORC production slightly increase from the first case, and then they both tend to flatten. The PB period of the CB decreases until an increase of the DH substation downsizing occurs, then it slightly increases due to the higher HP consumption, which is not entirely compensated by the slight increment of the ORC production (Table 6).

The same sensitivity analysis applied in the 2nd reference case (Fig. A8 of the Annex) accounts for the cost associated with the HP heat absorption. As a general conclusion, the CB techno-economic

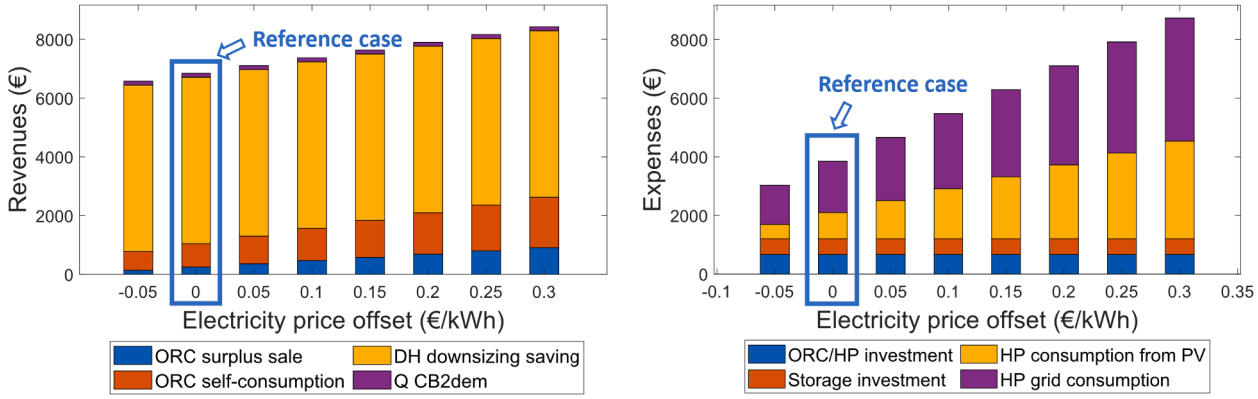

Fig. 14. Carnot battery annual revenues and expenses when varying the electricity price of an offset for the 1st reference case.

Table 8
Carnot battery payback period when varying the electricity price of an offset for the 1st reference case.

Electricity price offset (€/kWh)	−0.05	0	0.05	0.1	0.15	0.2	0.25	0.3
PB (years)	7.59	8.59	9.88	11.6	14.1	18.0	24.9	–
DPB (years)	8.81	10.2	12.2	15.1	20.0	30.2	–	–

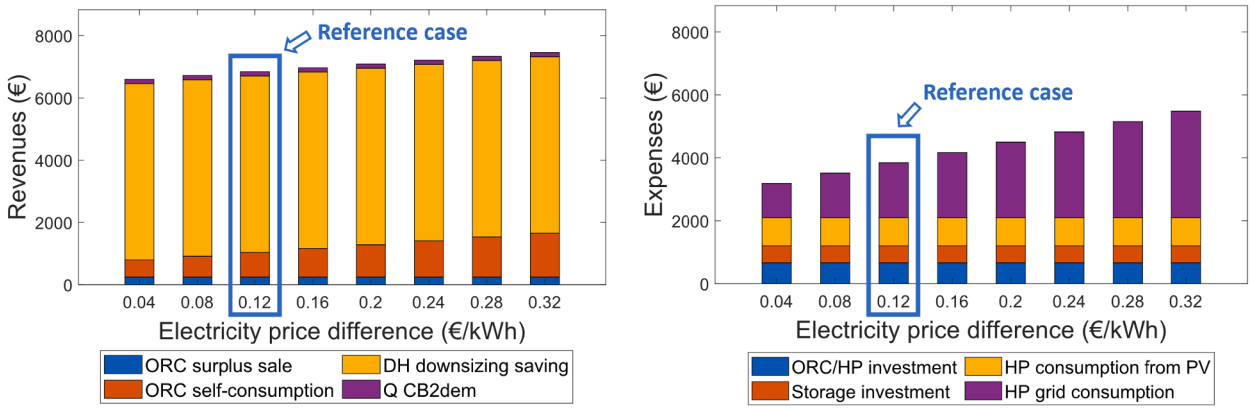

Fig. 15. Carnot battery annual revenues and expenses when varying the electricity price difference between purchasing and selling for the 1st reference case.

Table 9
Carnot battery payback period when varying the electricity price difference between purchasing and selling for the 1st reference case.

Electricity price difference (€/kWh)	0.04	0.08	0.12	0.16	0.20	0.24	0.28	0.32
PB (years)	7.83	8.19	8.59	9.02	9.51	10.0	10.6	11.3
DPB (years)	9.13	9.65	10.2	10.9	11.6	12.5	13.4	14.6

Table 10
Carnot battery payback period when varying the reversible HP/ORC specific investment cost.

HP/ORC investment cost (€/kW)	500	1000	1500	2000	2500	3000	3500	4000	4500	5000
PB (years)	5.02	6.21	7.40	8.59	9.77	11.1	12.2	13.3	14.5	15.7
DPB (years)	5.47	6.95	8.54	10.2	12.0	14.0	16.1	18.4	20.9	23.7

performance is rather insensitive to the PV panels surface. This is because the CB energetic performance is mostly dependent on the temperature levels, while the economic performance is strongly related to the DH substation downsizing, which is not affected by the renewable electricity production, especially when the possibility of absorbing electricity from the grid to run the HP is considered.

3.4. Effect of the thermal energy storage volume

Since the CB is classified as an energy storage and its capacity is strictly dependent on the TES volume, a sensitivity analysis varying the storage volume has been conducted, to investigate how it affects the overall performance and the economic convenience of the system. The storage volume has been varied from 7 to 16 m^3 with a step of 3 m^3. The results are discussed below only for the 1st case, while for the 2nd case please refer to Fig. A9 in the Annex.

Fig. 13 shows the annual revenues and expenses associated with the CB varying the storage volume. The increase of the TES capacity allows the storage of a greater amount of thermal energy that can be used to cover a higher part of the thermal demand peaks, further reducing the DH substation size and the associated investment costs. However, the DH downsizing does not increase monotonically with the storage volume (Table 7). It stops when the CB can cover the whole early morning peak, and further downsizing would require satisfying part of the thermal demand with the CB during the whole wintertime day. The HP consumption (from both PV production and grid) and the ORC production increase because the increment of the storage capacity allows the HP to produce a larger amount of thermal energy, which is then used for the thermal demand peak shaving and the ORC discharge phase. Furthermore, the annual expenses increase with the storage volume, also because of the increase of the investment cost. As shown in Table 7, the payback period decreases with the storage volume until a reduction of the DH substation size occurs, but, after that, it increases due to the higher investment cost of the storage, which is not compensated by a significant increase in the annual gain. Eventually, both the self-consumption and the self-production rates slightly increase, the first because of the increase of the HP consumption, the second due to the higher ORC production.

To conclude, there is an optimal storage size that minimizes the payback period for each application. In this case, the optimal storage size is 13 m^3, and it is the result of a compromise between the profit provided by a higher storage capacity and the increase in the investment costs. The optimal size is strictly dependent on both the CB nominal power and the intensity of the thermal demand peaks to be shaved.

3.5. Effect of the electricity price profiles

A further sensitivity analysis has been performed by varying the electricity price, simulating two scenarios. With the first scenario, the aim is to simulate an increase (or decrease) of the average electricity price, without affecting the difference ($\Delta price_{ref}$) between the purchasing and selling prices. Therefore, the purchasing and selling electricity price profiles are corrected of a certain offset (which corresponds to the variation of the average electricity price), according to Eq. (32).

$$\begin{aligned} C_{el,sale} &= reference\ spot\ market\ profile\ (2021) + offset \quad (€/kWh) \\ C_{el,pur} &= reference\ spot\ market\ profile\ (2021) + \Delta price_{ref} + offset \quad (€/kWh) \end{aligned} \tag{32}$$

Fig. 14 shows the annual revenues and expenses obtainable with the 1st reference case hypothesis but correcting the electricity price profiles according to Eq. (32). The DH substation downsizing is not influenced by the electricity price variation, so the associated gain results to be constant. Indeed, the DH substation downsizing profit is proportional to the DH fee, which is assumed as constant. Varying the average electricity price, both the ORC production revenues and HP consumption costs increase. However, the latter increases more than the former because the

HP consumption is always higher than the ORC production. Consequently, the increase in the average electricity price results in a reduction of the annual economic gain and an increase in the PB period (Table 8). Furthermore, if the DH fee and the thermal energy price are kept constant, the flexibility on the thermal side provided by the CB loses weight in the economic gain computation, when the electricity price increases.

The results for the 2nd reference case are shown in the Annex in Fig. A10, and follow the same trend of the results for the 1st case. The HP heat consumption does not vary with the electricity price because the HP energy consumption and the thermal energy price are constant.

The second scenario aims at simulating a variation in the price difference ($\Delta price$) between the electricity purchasing and selling price. Thus, in this scenario, the selling price profile is assumed fixed and always equal to the reference case profile, while the purchasing price is corrected varying the difference ($\Delta price$) with the selling price profile, according to Eq. (33).

$$\begin{aligned} C_{el,sale} &= reference\ spot\ market\ profile\ (2021) \quad (€/kWh) \\ C_{el,pur} &= reference\ spot\ market\ profile\ (2021) + \Delta price \quad (€/kWh) \end{aligned} \tag{33}$$

Fig. 15 shows the results of the sensitivity analysis for the 1st reference case when varying the electricity price difference ($\Delta price$) between the purchasing and selling profiles, according to Eq. (33). As in the previous analysis, the reduction of the DH size, the thermal demand covered by the CB and the CB investment cost remain constant. Furthermore, since the electricity price profile for sale does not vary in this sensitivity analysis, the ORC revenues due to the sale surplus and the HP renewable consumption result to be constant. The only economic indexes that increase are the revenues due to the ORC production for self-consumption and the expenses due to the HP grid consumption. Since the HP consumption is higher than the ORC production, when increasing the purchasing price, the expenses increase more than the revenues, resulting in a lower gain and higher PB period (Table 9). To conclude, in this case, the more the purchasing price is similar to the selling price, the higher the gain because most of the revenues come from the DH substation downsizing.

In the Annex, the results for the 2nd reference case are presented in Fig. A11. As a general conclusion for this subsection, an increase in the electricity price reduces the CB economic convenience (i) because the improved flexibility on the thermal side loses weight in the economic gain computation, and (ii) because the HP consumption costs increase more than the ORC production revenues.

3.6. Effect of the reversible heat pump/organic Rankine cycle specific investment cost

Eventually, a sensitivity analysis has been accomplished by varying the reversible HP/ORC specific investment cost from 500 to 5000 €/kW. The system investment cost is a fixed cost (capital expenditure), therefore it does not influence the scheduling and the operation of the CB in the integrated system. As a result, the CB yearly gain, which is determined by the operating cost, is not affected by a change in the system investment cost, which has an impact only on the simple and discounted payback period. Table 10 shows the PB and DPB period obtained by varying the reversible HP/ORC specific investment cost and considering the storage investment cost as constant.

Even though the CB investment cost is a parameter that does not influence the control strategy developed and presented in this work, it strongly affects the economic feasibility of the proposed integration. Heat pump and organic Rankine cycle are mature and well-known technologies, so the limitations from the commercial point of view are mostly related to the investment cost.

4. Conclusions

This study aims to present a detailed rule-based control strategy to schedule the operation of a 10 kWe-size reversible HP/ORC Carnot battery in an integrated system, composed of a DH substation and a PV power plant, to satisfy a user's thermal and electric demand. The control strategy is defined to maximize the economic benefit obtainable through the CB intervention in the integrated system during annual operation, considering the daily variation of the electricity spot market price. The thermal energy stored in the CB allows for shaving the early morning peaks occurring in the thermal demand, allowing for a significant downsizing of the DH substation, with considerable savings in the investment costs. The CB off-design model is based on a semi-empirical approach, it is validated on the test-bench available at the Thermodynamics Laboratory of the University of Liège, and it is rescaled to 10 kWe. Variable boundary conditions are assumed to evaluate the overall performance. The user electric and thermal energy profiles derive from data collected in a building of the University of Liège campus, the solar irradiance and ambient temperature profiles are ones registered in Liège during the year 2020, and the electricity price derives from the Belgian spot market profile in 2021. Furthermore, two cases of the reference system, different for the HP cold source, are analysed. In the first case, the HP absorbs thermal energy from free waste heat at a constant temperature, which is assumed to be always available and completely free of charge. In the second case, the HP evaporator absorbs thermal energy from the return branch of the DH substation, so there is an additional cost for it.

The main findings of this work are summarized as follows:

- According to the simulation results, in the 1st reference case, a significant part of the revenues is provided by the reduction of the DH substation size, which is 47 %, allowing savings of about 5000 € per year. The self-consumption and production rates show that there is an increase of 6 %, in the electricity demand covered by the renewable production, and 18 % in the renewable production consumed by the user. Concerning the reversible HP/ORC Carnot battery, a yearly average COP of 4.8 is reached by the HP, while the ORC average discharge efficiency is about 8.4 %. From the economic point of view, the CB results to have a payback period of less than 9 years.
- In the 2nd reference case, the HP is not allowed to work when the thermal discharge mode occurs because the DH substation is already exploited at its nominal power. Thus, the HP is not allowed to provide a booster to the TES, penalizing the DH substation downsizing and the associated economic gain. In this case, the CB integration does not provide a positive gain.
- Some control rules adopted in the strategy are discussed, proving the improvement they add to the control strategy. Letting the ORC discharge the storage as soon as possible, without waiting for a higher electricity price within the day, and allowing the HP to absorb electricity from the grid also when the price is high, reduces the gain and increases the CB payback period to about 11 years. This shows the importance of an optimal management of the system for profit maximization.
- Also removing the possibility of purchasing electricity from the grid to feed the HP further reduces the gain because it affects the DH substation downsizing. In case of low or absent solar radiation, the thermal production through the HP is penalized resulting in less thermal energy to shave the peaks. In this case, the PB period is assessed to be about 12.6 years.
- Sensitivity analysis varying the PV power plant surface area and the storage volume are presented. Results show that the PV panels area does not significantly affect the gain and the CB operation, because the energetic performance is mainly dependent on the temperature levels, while the economic gain is strongly related to the DH substation downsizing, not affected by the renewable electricity

production when the possibility of absorbing electricity from the grid to run the HP is considered. Differently, an increase in the storage volume strongly influences the DH substation downsizing and the other revenues and expenses. However, since when increasing the storage volume, both revenues and expenses increase, a strong variation in the economic gain and PB period cannot be observed. The minimum PB period is observed for a storage volume of 13 m^3, which results to be the optimal size for the analysed application.

- A sensitivity analysis is also performed correcting the electricity price profile of a certain offset, increasing and decreasing the average value. Two scenarios, one in which both the purchasing and selling price profiles are varied and one in which only the purchasing price profile is varied, are analysed. In both the scenarios, even if with different intensities, an increase in the electricity price results in a decrease in the economic gain. The reasons lie in the fact that the HP expenses are much higher than the ORC revenues (the HP consumption is much higher than the ORC production) because the HP mostly works to produce thermal energy that will be addressed to shave the thermal demand peaks. Therefore, when the electricity price increases, the HP electricity expenses increase, while the benefit provided by the DH substation downsizing remains constant because it is not affected by the electricity price.

The rule-based control strategy approach, developed to manage the CB operation in an integrated system and presented in this work, can be transferred also to different applications. The specific nature of the approach requires to modify the rules to fit the characteristics of a different case study, but the overall approach can be easily exported. Indeed, the Authors presented a techno-economical assessment of a thermally integrated reversible HP/ORC CB applied to a data center cooling system. A similar rule-based management strategy was developed to maximize the economic gain obtainable by including the CB in the integrated system. Since the requirements and energy flows are different in the two applications, the rules and the priorities in the procedure decisions were modified. However, the structure of the problem, with the economic function calculated at each time step, and the approach adopted to formulate the rules are the same in the two case studies.

4.1. Future developments

The future perspectives involve different developments. The main ones, some already planned, are presented below:

- The control strategy, described and numerically implemented in this study, will be transferred and integrated into the control and acquisition system of a new 10 kWe-sized prototype of reversible HP/ORC Carnot battery, which is being built in the Thermodynamics Laboratory of the University of Liège. The new prototype will be directly connected to the DH substation of the lab to provide thermal integration. After that, a wide experimental campaign will be conducted to completely characterize the Carnot battery test bench and validate the control strategy, to identify guidelines to develop efficient Carnot batteries in the future.
- A simplified model of the system will be developed to investigate the techno-economic performance of a Carnot battery through a more robust optimization tool, based on mixed linear integer programming.
- Regarding the modelling accuracy, variable PV modules efficiency could be considered to assess its impact on the yearly distribution of the operating costs.
- Concerning a further improvement of the described rule-based control strategy, it could be interesting to analyse if, when a higher difference between the electricity price for selling and purchasing occurs, a lower reduction of the DH substation (due to the removal of the possibility of feeding the HP with electricity from the grid) can be economically convenient.
- In future works, other case studies could be analysed to enlarge the set of applications in which Carnot batteries could improve the flexibility in heat and power production, and the match with the user's demands. Furthermore, different configurations of Carnot batteries may be interesting for future applications: an example could be recovering the heat discharged at the ORC condenser to cover a very low-temperature thermal demand, and to use a high-temperature DH network as the HP cold source.

CRediT authorship contribution statement

Chiara Poletto: Methodology, Software, Formal analysis, Investigation, Writing – original draft. **Olivier Dumont:** Conceptualization, Investigation, Data curation, Writing – review & editing, Supervision. **Andrea De Pascale:** Resources, Writing – review & editing, Supervision. **Vincent Lemort:** Resources, Writing – review & editing. **Saverio Ottaviano:** Writing – review & editing. **Olivier Thomé:** Writing – review & editing.

Declaration of competing interest

The authors declare that they have no known competing financial interests or personal relationships that could have appeared to influence the work reported in this paper.

Data availability

Data will be made available on request.

Acknowledgement

The work documented in this publication has been funded by the 2021 Scholarship of the Knowledge Center on Organic Rankine Cycle technology (www.kcorc.org). The results were obtained by the collaboration of the Thermodynamics Laboratory of the University of Liège, Belgium, and the Department of Industrial Engineering of the University of Bologna, Italy.

Funding Sources

This research did not receive any specific grant from funding agencies in the public, commercial, or not-for-profit sectors.

Annex.

The annex contains further figures and graphs.

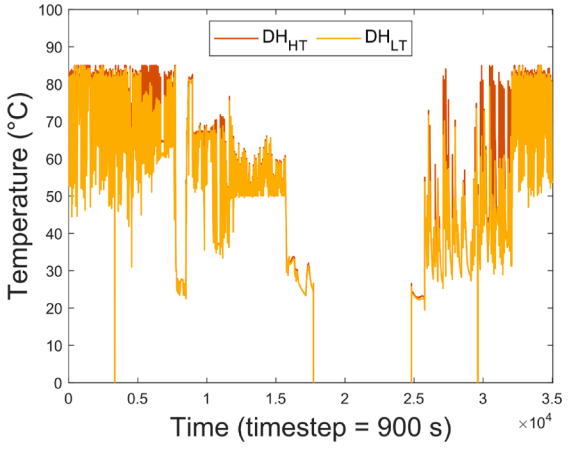

Fig. A1. DH supply (HT) and return (LT) branches temperature.

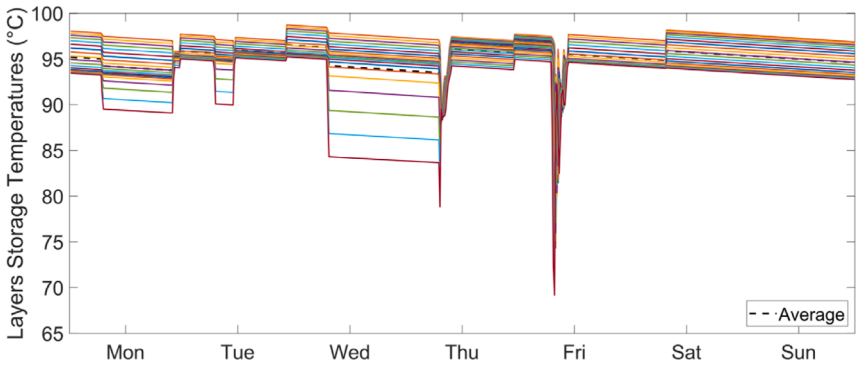

Fig. A2. Storage temperature profile in a week in winter.

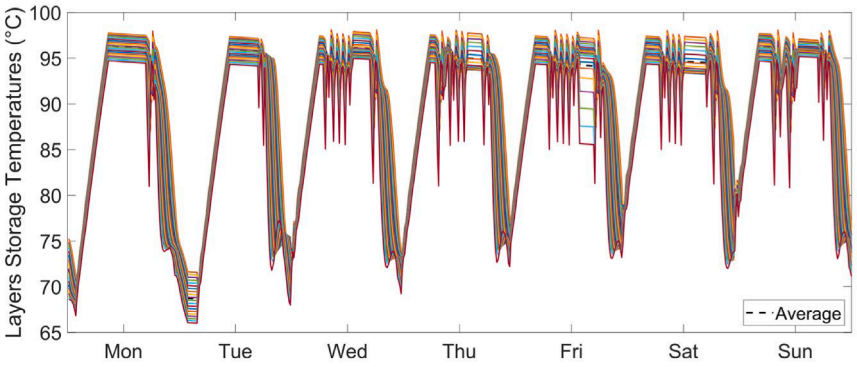

Fig. A3. Storage temperature profile in a week in summer.

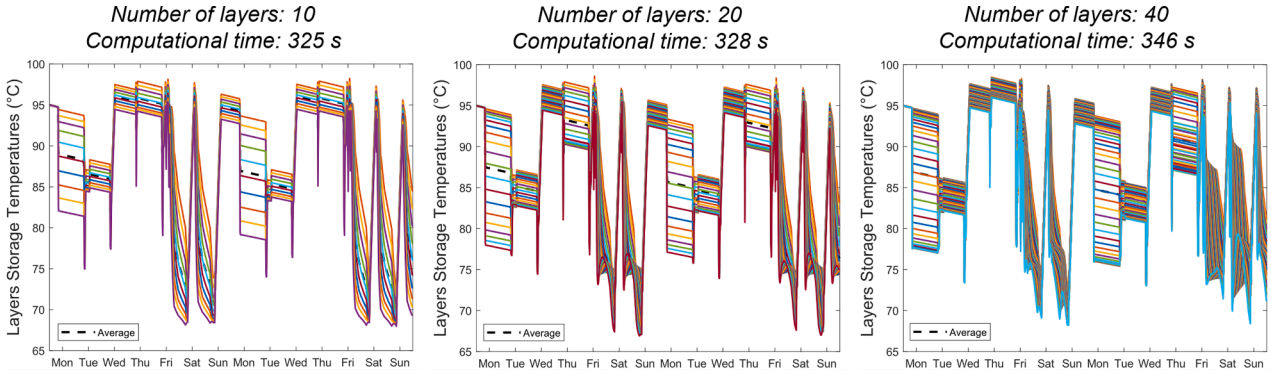

Fig. A4. Two weeks storage temperature profile and computational time varying the volume number of discretization layers.

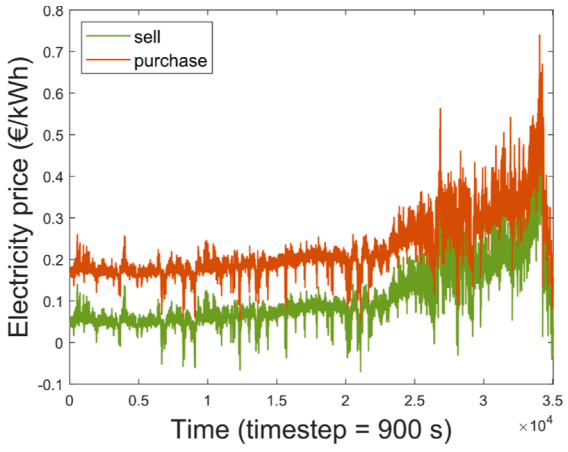

Fig. A5. Electricity price profiles.

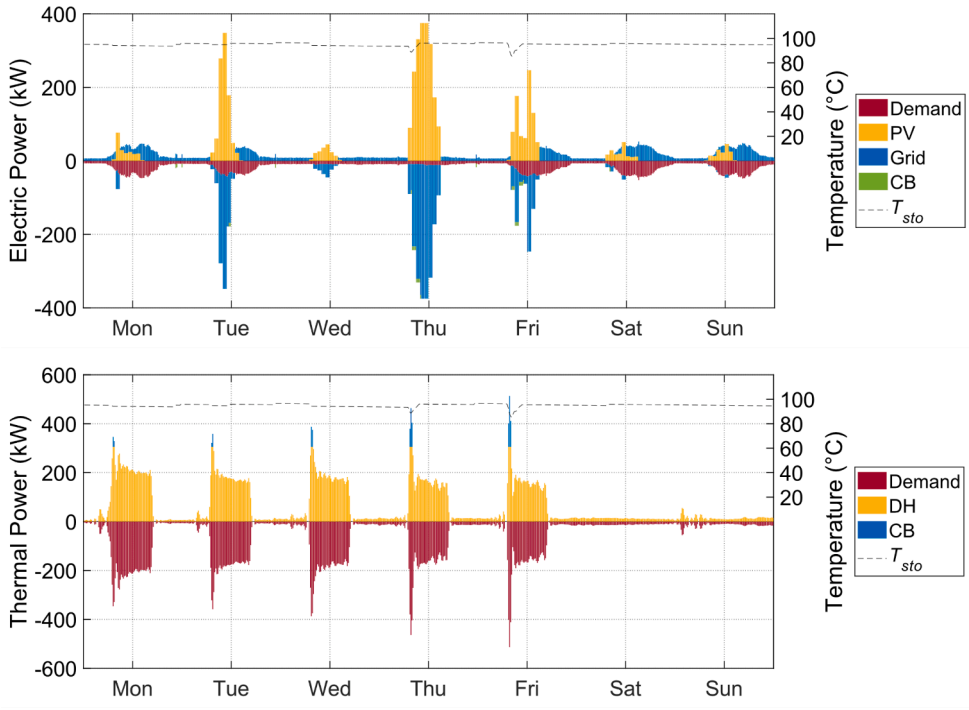

Fig. A6. Electric and thermal power profile in a general week in winter.

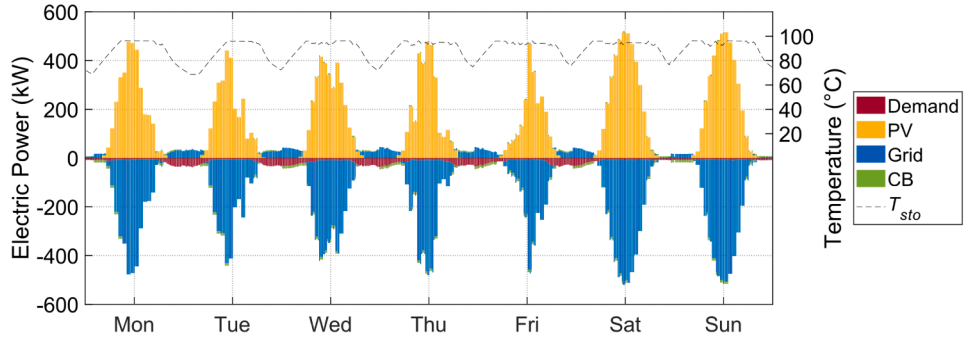

Fig. A7. Electric power profile in a general week in summer.

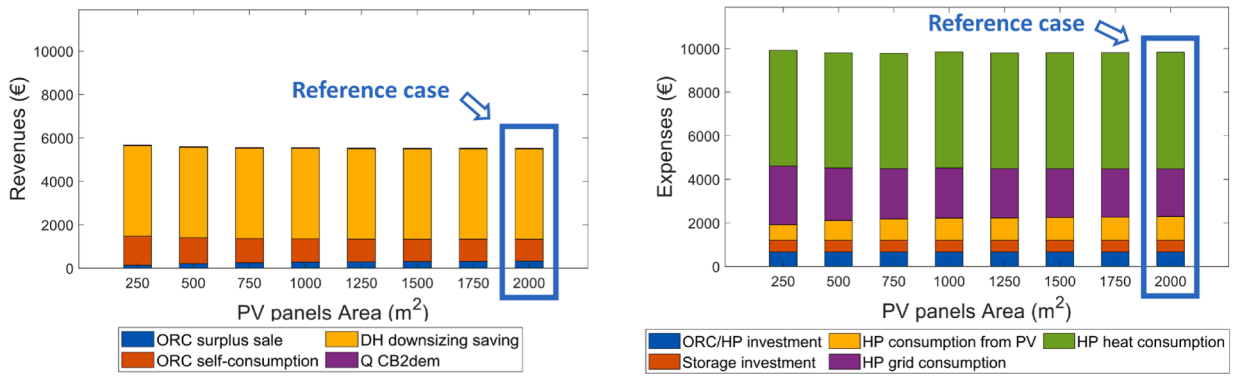

Fig. A8. Carnot battery annual revenues and expenses when varying the PV surface for the 2nd reference case.

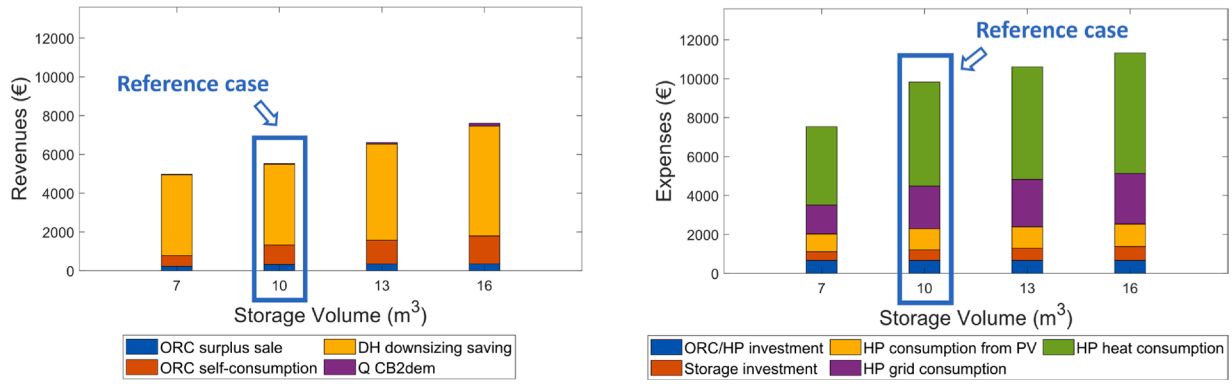

Fig. A9. Carnot battery annual revenues and expenses when varying the storage volume for the 2nd reference case.

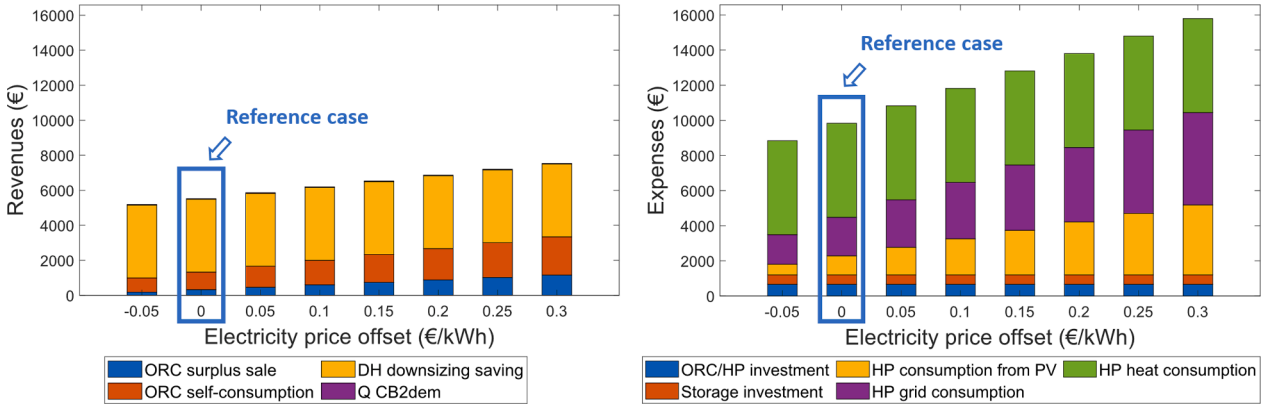

Fig. A10. Carnot battery annual revenues and expenses when varying the electricity price of an offset for the 2nd reference case.

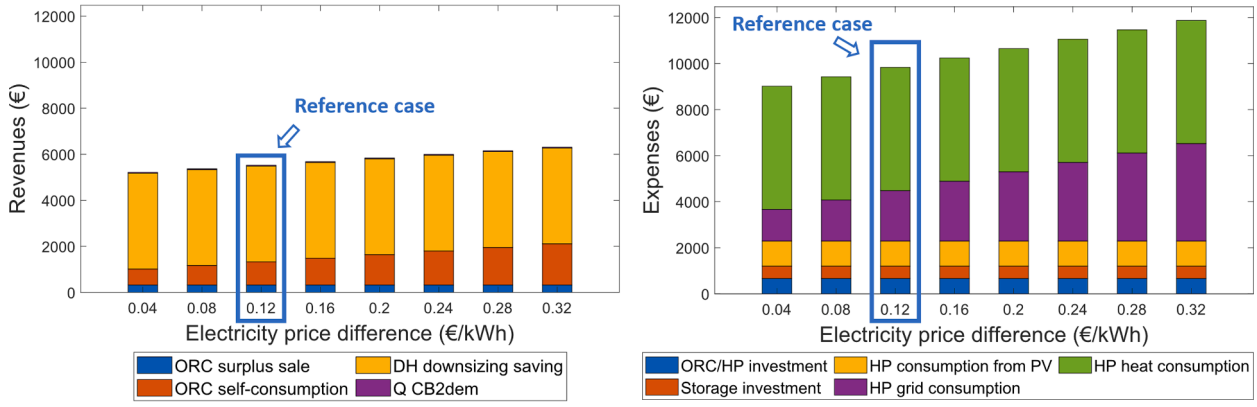

Fig. A11. Carnot battery annual revenues and expenses when varying the electricity price difference between purchasing and selling for the 2nd reference case.

References

[1] Bouckaert S. et al., Net Zero by 2050: A Roadmap for the Global Energy Sector, 2021, Accessed: Oct. 28, 2022. [Online]. Available: https://trid.trb.org/view/1856381.

[2] "2050 long-term strategy." Accessed: Oct. 28, 2022. [Online]. Available: https://climate.ec.europa.eu/eu-action/climate-strategies-targets/2050-long-term-strategy_en.

[3] Vecchi A, et al. Carnot Battery development: A review on system performance, applications and commercial state-of-the-art. J Energy Storage Nov. 2022;55:105782. https://doi.org/10.1016/j.est.2022.105782.

[4] Zühlsdorf B, Bühler F, Bantle M, Elmegaard B. Analysis of technologies and potentials for heat pump-based process heat supply above 150 °C. Energy Convers Manag X Apr. 2019;2:100011. https://doi.org/10.1016/j.ecmx.2019.100011.

[5] Lai CS, McCulloch MD. Levelized cost of electricity for solar photovoltaic and electrical energy storage. Appl Energy Mar. 2017;190:191–203. https://doi.org/10.1016/j.apenergy.2016.12.153.

[6] Song Z, et al. Multi-objective optimization of a semi-active battery/supercapacitor energy storage system for electric vehicles. Appl Energy Dec. 2014;135:212–24. https://doi.org/10.1016/j.apenergy.2014.06.087.

[7] Díaz-González F, Sumper A, Gomis-Bellmunt O, Bianchi FD. Energy management of flywheel-based energy storage device for wind power smoothing. Appl Energy Oct. 2013;110:207–19. https://doi.org/10.1016/j.apenergy.2013.04.029.

[8] Massaro MC, Biga R, Kolisnichenko A, Marocco P, Monteverde AHA, Santarelli M. Potential and technical challenges of on-board hydrogen storage technologies coupled with fuel cell systems for aircraft electrification. J Power Sources Jan. 2023;555:232397. https://doi.org/10.1016/j.jpowsour.2022.232397.

[9] Hendrick P. Introduction to Hydro Energy Storage. In: Cabeza LF, editor. Encyclopedia of Energy. Oxford: Elsevier; 2022. p. 100–3. https://doi.org/10.1016/B978-0-12-819723-3.00158-X.

[10] Han Y, Cui H, Ma H, Chen J, Liu N. Temperature and pressure variations in salt compressed air energy storage (CAES) caverns considering the air flow in the underground wellbore. J Energy Storage Aug. 2022;52:104846. https://doi.org/10.1016/j.est.2022.104846.

[11] Barbour ER, Pottie DLF. Adiabatic compressed air energy storage systems. In: Cabeza LF, editor. Encyclopedia of Energy. Oxford: Elsevier; 2022. p. 188–203. https://doi.org/10.1016/B978-0-12-819723-3.00061-5.

[12] Vecchi A, Li Y, Ding Y, Mancarella P, Sciacovelli A. Liquid air energy storage (LAES): A review on technology state-of-the-art, integration pathways and future perspectives. Adv Appl Energy Aug. 2021;3:100047. https://doi.org/10.1016/j.adapen.2021.100047.

[13] Dumont O, Frate GF, Pillai A, Lecompte S, De paepe M, Lemort V. Carnot battery technology: A state-of-the-art review. J. Energy Storage, vol. 32, p. 101756, Dec. 2020, doi: 10.1016/j.est.2020.101756.

[14] Gimeno-Gutiérrez M, Lacal-Arántegui R. Assessment of the European potential for pumped hydropower energy storage based on two existing reservoirs. Renew Energy Mar. 2015;75:856–68. https://doi.org/10.1016/j.renene.2014.10.068.

[15] Frate GF, Ferrari L, Desideri U. Multi-criteria investigation of a pumped thermal electricity storage (PTES) system with thermal integration and sensible heat storage. Energy Convers Manag Mar. 2020;208:112530. https://doi.org/10.1016/j.enconman.2020.112530.

[16] Dumont O, Lemort V. Mapping of performance of pumped thermal energy storage (Carnot battery) using waste heat recovery. Energy Nov. 2020;211:118963. https://doi.org/10.1016/j.energy.2020.118963.

[17] Ökten K, Kurşun B. Thermo-economic assessment of a thermally integrated pumped thermal energy storage (TI-PTES) system combined with an absorption refrigeration cycle driven by low-grade heat source. J Energy Storage Jul. 2022;51:104486. https://doi.org/10.1016/j.est.2022.104486.

[18] Frate GF, Antonelli M, Desideri U. A novel Pumped Thermal Electricity Storage (PTES) system with thermal integration. Appl Therm Eng Jul. 2017;121:1051–8. https://doi.org/10.1016/j.applthermaleng.2017.04.127.

[19] Su Z, Yang L, Song J, Jin X, Wu X, Li X. Multi-dimensional comparison and multi-objective optimization of geothermal-assisted Carnot battery for photovoltaic load shifting. Energy Convers Manag Aug. 2023;289:117156. https://doi.org/10.1016/j.enconman.2023.117156.

[20] Zhang X, et al. The Carnot batteries thermally assisted by the steam extracted from thermal power plants: A thermodynamic analysis and performance evaluation. Energy Convers Manag Dec. 2023;297:117724. https://doi.org/10.1016/j.enconman.2023.117724.

[21] Xia R, et al. Comprehensive performance analysis of cold storage Rankine Carnot batteries: Energy, exergy, economic, and environmental perspectives. Energy Convers Manag Oct. 2023;293:117485. https://doi.org/10.1016/j.enconman.2023.117485.

[22] Bellos E. Thermodynamic analysis of a Carnot battery unit with double exploitation of a waste heat source. Energy Convers Manag Jan. 2024;299:117844. https://doi.org/10.1016/j.enconman.2023.117844.

[23] Torricelli N, Branchini L, De Pascale A, Dumont O, Lemort V. Optimal Management of Reversible Heat Pump/Organic Rankine Cycle Carnot Batteries. J Eng. Gas Turbines Power, 145 (4) 2023, doi: 10.1115/1.4055708.

[24] Bianchi M, et al. Experimental analysis of a micro-ORC driven by piston expander for low-grade heat recovery. Appl Therm Eng Feb. 2019;148:1278–91. https://doi.org/10.1016/j.applthermaleng.2018.12.019.

[25] Eppinger B, Steger D, Regensburger C, Karl J, Schlücker E, Will S. Carnot battery: Simulation and design of a reversible heat pump-organic Rankine cycle pilot plant. Appl Energy Apr. 2021;288:116650. https://doi.org/10.1016/j.apenergy.2021.116650.

[26] Dumont O, Lemort V. Thermo-technical approach to characterize the performance of a reversible heat pump/organic Rankine cycle power system depending on its operational conditions. ECOS 2019. 2019.

[27] Abarr M, Hertzberg J, Montoya LD. Pumped Thermal Energy Storage and Bottoming System Part B: Sensitivity analysis and baseline performance. Energy Jan. 2017;119:601–11. https://doi.org/10.1016/j.energy.2016.11.028.

[28] Yu X, Qiao H, Yang B, Zhang H. Thermal-economic and sensitivity analysis of different Rankine-based Carnot battery configurations for energy storage. Energy Convers Manag May 2023;283:116959. https://doi.org/10.1016/j.enconman.2023.116959.

[29] [Online]. Available: https://users.ugent.be/~slecompt/carnot_battery.htm.

[30] Niu J, Wang J, Liu X, Dong L. Optimal integration of solar collectors to Carnot battery system with regenerators. Energy Convers Manag Feb. 2023;277:116625. https://doi.org/10.1016/j.enconman.2022.116625.

[31] Tassenoy R, Couvreur K, Beyne W, De Paepe M, Lecompte S. Techno-economic assessment of Carnot batteries for load-shifting of solar PV production of an office building. Renew Energy Nov. 2022;199:1133–44. https://doi.org/10.1016/j.renene.2022.09.039.

[32] Lin X, Sun P, Zhong W, Wang J. Thermodynamic analysis and operation investigation of a cross-border integrated energy system based on steam Carnot battery. Appl Therm Eng Feb. 2023;220:119804. https://doi.org/10.1016/j.applthermaleng.2022.119804.

[33] Scharrer D, Bazan P, Pruckner M, German R. Simulation and analysis of a Carnot Battery consisting of a reversible heat pump/organic Rankine cycle for a domestic application in a community with varying number of houses. Energy Dec. 2022;261:125166. https://doi.org/10.1016/j.energy.2022.125166.

[34] "The Project » CHESTER Project," CHESTER Project. Accessed: Jan. 25, 2023. [Online]. Available: https://www.chester-project.eu/about-chester/the-project/.

[35] "CHESTER_D6.2_Business-cases-definition-and-baseline-for-Business-models.".

[36] "CHESTER-D6.6-Market-replicability-potential.pdf." [Online]. Available: https://www.chester-project.eu/wp-content/uploads/2023/02/CHESTER-D6.6-Market-replicability-potential.pdf.

[37] Dumont O, Reyes A, Lemort V. Modelling of a thermally integrated Carnot battery using a reversible heat pump/organic Rankine cycle. presented at the ecos conference. 2020.

[38] Dumont O. Investigation of a heat pump reversible into an organic Rankine cycle and its application in the building sector. PhD Dissertation 2017.

[39] Ancona MA, et al. Solar driven micro-ORC system assessment for residential application. Renew Energy Aug. 2022;195:167–81. https://doi.org/10.1016/j.renene.2022.06.007.

[40] Dickes R, Dumont O, Daccord R, Quoilin S, Lemort V. Modelling of organic Rankine cycle power systems in off-design conditions: An experimentally-validated comparative study. Energy Mar. 2017;123:710–27. https://doi.org/10.1016/j.energy.2017.01.130.

[41] Lemort V. Contribution to the characterization of scroll machines in compressor and expander modes. University of Liège; 2008.

[42] Landelle A, Tauveron N, Revellin R, Haberschill P, Colasson S, Roussel V. Performance investigation of reciprocating pump running with organic fluid for organic Rankine cycle. Appl Therm Eng Feb. 2017;113:962–9. https://doi.org/10.1016/j.applthermaleng.2016.11.096.

[43] Dumont O, Charalampidis A, Lemort V. Experimental Investigation Of A Thermally Integrated Carnot Battery Using A Reversible Heat Pump/Organic Rankine Cycle. Int. Refrig. Air Cond. Conf., May 2021, [Online]. Available: https://docs.lib.purdue.edu/iracc/2085.

[44] Powell KM, Edgar TF. An adaptive-grid model for dynamic simulation of thermocline thermal energy storage systems. Energy Convers Manag Dec. 2013;76:865–73. https://doi.org/10.1016/j.enconman.2013.08.043.

[45] Nash AL, Badithela A, Jain N. Dynamic modeling of a sensible thermal energy storage tank with an immersed coil heat exchanger under three operation modes. Appl Energy Jun. 2017;195:877–89. https://doi.org/10.1016/j.apenergy.2017.03.092.

[46] Patankar S. Numerical Heat Transfer and Fluid Flow. Boca Raton: CRC Press 2018. https://doi.org/10.1201/9781482234213.

[47] "JRC Photovoltaic Geographical Information System (PVGIS) - European Commission." Accessed: Feb. 10, 2023. [Online]. Available: https://re.jrc.ec.europa.eu/pvg_tools/it/#MR.

[48] Kang A, Korolija I, Rovas D. Photovoltaic Thermal District Heating: A review of the current status, opportunities and prospects. Appl Therm Eng Nov. 2022;217:119051. https://doi.org/10.1016/j.applthermaleng.2022.119051.

[49] Obalanlege MA, Mahmoudi Y, Douglas R, Ebrahimnia-Bajestan E, Davidson J, Bailie D. Performance assessment of a hybrid photovoltaic-thermal and heat pump system for solar heating and electricity. Renew Energy Apr. 2020;148:558–72. https://doi.org/10.1016/j.renene.2019.10.061.

[50] Mi P, Zhang J, Han Y, Guo X. Study on energy efficiency and economic performance of district heating system of energy saving reconstruction with photovoltaic thermal heat pump. Energy Convers Manag Nov. 2021;247:114677. https://doi.org/10.1016/j.enconman.2021.114677.

[51] Parra D, Walker GS, Gillott M. Are batteries the optimum PV-coupled energy storage for dwellings? Techno-economic comparison with hot water tanks in the UK. Energy Build Mar. 2016;116:614–21. https://doi.org/10.1016/j.enbuild.2016.01.039.

[52] Pakere I, Lauka D, Blumberga D. Solar power and heat production via photovoltaic thermal panels for district heating and industrial plant. Energy Jul. 2018;154:424–32. https://doi.org/10.1016/j.energy.2018.04.138.

[53] Bell IH, Wronski J, Quoilin S, Lemort V. Pure and Pseudo-pure Fluid Thermophysical Property Evaluation and the Open-Source Thermophysical Property Library CoolProp. Ind. Eng. Chem. Res., vol. 53, no. 6, Art. no. 6, Feb. 2014, doi: 10.1021/ie4033999.

[54] Yuan X, Liang Y, Hu X, Xu Y, Chen Y, Kosonen R. Waste heat recoveries in data centers: A review. Renew Sustain Energy Rev Dec. 2023;188:113777. https://doi.org/10.1016/j.rser.2023.113777.

[55] Villasmil W, Fischer LJ, Worlitschek J. A review and evaluation of thermal insulation materials and methods for thermal energy storage systems. Renew Sustain Energy Rev Apr. 2019;103:71–84. https://doi.org/10.1016/j.rser.2018.12.040.

[56] Lemmens S. Cost Engineering Techniques and Their Applicability for Cost Estimation of Organic Rankine Cycle Systems. Energies, vol. 9, no. 7, Art. no. 7, Jul. 2016, doi: 10.3390/en9070485.

[57] Shamoushaki M, Niknam PH, Talluri L, Manfrida G, Fiaschi D. Development of cost correlations for the economic assessment of power plant equipment. Energies 2021;14(9). https://doi.org/10.3390/en14092665.

[58] Dumont O, Carmo C, Georges E, Quoilin S, Lemort V. Economic assessment of electric energy storage for load shifting in positive energy building. Int J Energy Environ Eng Mar. 2017;8(1):25–35. https://doi.org/10.1007/s40095-016-0224-2.

[59] Résimont MT. Strategic outline and sizing of district heating networks using a geographic information system." Accessed: Apr. 18, 2023. [Online]. Available: https://www.fsa.uliege.be/cms/c_7790914/en/strategic-outline-and-sizing-of-district-heating-networks-using-a-geographic-information-system.

[60] "Market data." Accessed: Feb. 10, 2023. [Online]. Available: https://www.nordpoolgroup.com/en/Market-data1/Dayahead/Area-Prices/be/hourly/.
[61] Baetens R, et al. Assessing electrical bottlenecks at feeder level for residential net zero-energy buildings by integrated system simulation. Appl Energy Aug. 2012;96:74–83. https://doi.org/10.1016/j.apenergy.2011.12.098.
[62] Lecompte S. Performance evaluation of organic Rankine cycle architectures : application to waste heat valorisation, dissertation, Ghent University, 2016. Accessed: Mar. 09, 2023. [Online]. Available: http://hdl.handle.net/1854/LU-7223134.